NJC

PAPER

View Article Online
View Journal | View Issue

Cite this: *New J. Chem.*, 2014, **38**, 1611

Effect of N-donor ancillary ligands on structural and magnetic properties of oxalate copper(II) complexes†

Anna Świtlicka-Olszewska,[a] Barbara Machura,*[a] Jerzy Mroziński,[b] Bożena Kalińska,[b] Rafał Kruszynski[c] and Mateusz Penkala[d]

Received (in Victoria, Australia) 6th December 2013, Accepted 29th January 2014

DOI: 10.1039/c3nj01541f

www.rsc.org/njc

Through varying the auxiliary N-donor ligands under similar synthetic conditions nine new compounds: $[Cu(C_2O_4)(pz)]_n$ (**1**), $[Cu(C_2O_4)(apz)_2]_n\cdot(3H_2O)_n$ (**2**), $[Cu_2(\mu\text{-}C_2O_4)_2(H_2O)_2(ampz)_4]$ (**3**), $[Cu(C_2O_4)(mpz)_2]_n$ (**4**), $[Cu(C_2O_4)(aind)_2]_n$ (**5**), $[Cu_2(C_2O_4)_2(bpzm)_2]_n\cdot(3.5H_2O)_n$ (**6**), $[Cu(C_2O_4)(ampy)(H_2O)]_n$ (**7**) $\{[Cu_2(\mu\text{-}C_2O_4)(aepy)_2]\text{-}[Cu(C_2O_4)_2(H_2O)_2]\}_n\cdot(2H_2O)_n$ (**8**) and $[Cu_4(\mu\text{-}C_2O_4)_3(aepy)_4(H_2O)_2]Cl_2$ (**9**) (pz = pyrazole, apz = 3(5)-aminopyrazole, mpz = 3(5)-methylpyrazole, ampz = 3(5)-amino-5(3)-methylpyrazole, aind = 7-azaindole, bpzm = bis(pyrazol-1-yl)methane, ampy = 2-aminomethylpyridine and aepy = 2-(2-pyridyl)ethylamine) have been synthesized and characterised structurally (by single crystal X-ray analysis) and spectroscopically. On the basis of structural data, the influence of neutral N-donor ligands on the control of the final complex structures and the role of weak intermolecular interactions in the creation of molecular architectures have been discussed in detail. The two independent oxalate anions in **1**, adopting μ_3-oxalato-1κ^2O^1,O^2:2κO^1:3κO^{2a} and a relatively rare μ_4-oxalato-1κ^2O^1,O^2:2κO^1:3κO^{1a},O^{2a}:4κO^{2a} coordination mode, connect the Cu centers into a two-dimensional net extending along the crystallographic plane (100). Simultaneous existence of both amino and methyl groups in the ampz ligand results in the formation of a 0D dimeric structure of **3**. Compounds **2** and **4–8** display one-dimensional coordination structures, and the most significant differences between these structures concern the geometry around the copper(II) center and the coordination mode of the oxalate bridge. The structures of **2–9** are stabilized by the extensive hydrogen-bonding interactions that give rise to the supramolecular architectures. Additionally, the magnetic properties of the complexes **1–9** have been investigated and discussed in the context of their structures.

Introduction

The crystal engineering of inorganic–organic hybrid coordination polymers is currently one of the most active fields in coordination chemistry, supramolecular and materials chemistry. These compounds attract significant attention due to their intriguing architectures and topologies and due to their diverse promising applications. The inorganic component is the source of useful magnetic or optical properties, mechanical hardness, and thermal stability, while the organic component may offer processability, structural diversity and luminescent properties. The combination of the characteristics of the organic and inorganic components allows us to obtain new materials with potential applications in catalysis, separation, sorption, luminescence, biological chemistry, *etc.*[1]

The common strategy for synthesis of inorganic–organic hybrid coordination polymers is based upon the self-assembly strategy of organic ligands and metal ions. In this method the final structure and topology of a coordination polymer is a result of combination of various forces including strong and directional interactions (metal–ligand coordination bond) and much weaker interactions such as hydrogen bonds, π–π stacking, halogen–halogen and C–H···X (X = O, N, Cl or I *etc.*) contacts. To some extent, the coordination network assembly process can also be affected by counter anions, the ligand–metal molar ratio, coexisting neutral ligands, temperature, pH, and solvents used for crystallization. So far a variety of metal coordination frameworks with various topologies and properties have been synthesized and notable

[a] *Department of Crystallography, Institute of Chemistry, University of Silesia, 9th Szkolna St., 40-006 Katowice, Poland. E-mail: basia@ich.us.edu.pl*
[b] *Faculty of Chemistry, Wroclaw University, F. Joliot-Curie 14 St., 50-383 Wrocław, Poland. E-mail: jmroz@wchuwr.chem.uni.wroc.pl*
[c] *Department of X-ray Crystallography and Crystal Chemistry, Institute of General and Ecological Chemistry, Lodz University of Technology, 116 Żeromski St., 90-924 Łódź, Poland. E-mail: rafal.kruszynski@p.lodz.pl*
[d] *Department of Inorganic, Organometallic Chemistry and Catalysis, Institute of Chemistry, University of Silesia, 9th Szkolna St., 40-006 Katowice, Poland*

† Electronic supplementary information (ESI) available: Selected bond lengths and angles, short intra- and intermolecular contacts, powder XRD patterns and EPR spectra. CCDC 951616–951624. For crystallographic data in CIF or other electronic format see DOI: 10.1039/c3nj01541f

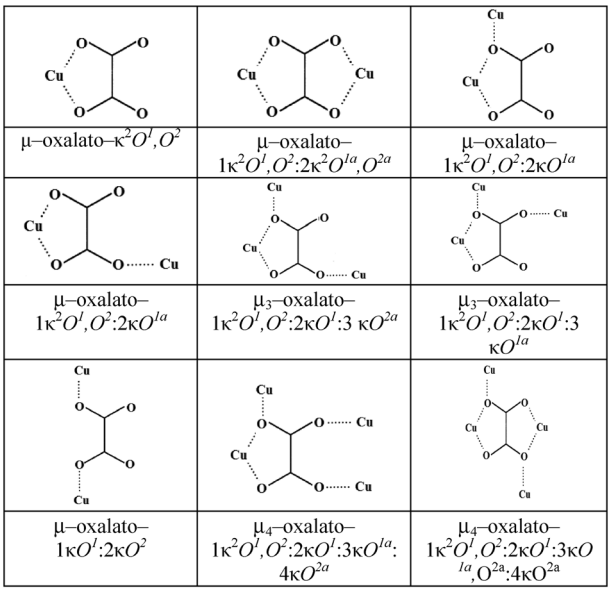

Scheme 1 Coordination modes observed for the oxalate groups in copper(II) complexes.

advances have been made in understanding the factors that influence network topology.‡

However, the rational control in the construction of polymeric networks remains a great challenge in crystal engineering and much more work is required to extend our knowledge of cooperative interactions between metal atoms and organic ligand moieties.[2]

Oxalate ions have been proven to be good connectors to bind to metal joints and play a key role in the design of new functional coordination networks. They have presented highly versatile binding modes (Scheme 1) and also serve as good hydrogen-bonding participants to give rise to higher dimensional structures. On the other hand, oxalate bridges act as efficient mediators of the magnetic interaction between the paramagnetic transition metal centers providing a great opportunity to develop new magnetic materials and explore systematically magneto-structural correlations.[3]

The aim of this research was to examine the role of N-donor ligands in structure formation of oxalate copper(II) complexes. For the study, we choose pyrazole derivatives and chelating ligands with an aromatic N-heterocycle ring and an aliphatic amine donor (Scheme 2). Except for bis(pyrazol-1-yl)methane, all these ligands contain hydrogen-bonding functionalities which can give rise to a broad variety of supramolecular networks.

Herein, nine oxalate copper(II) complexes, namely $[Cu(C_2O_4)(pz)]_n$ (**1**), $[Cu(C_2O_4)(apz)_2]_n\cdot(3H_2O)_n$ (**2**), $[Cu_2(\mu\text{-}C_2O_4)_2(H_2O)_2(ampz)_4]$ (**3**), $[Cu(C_2O_4)(mpz)_2]_n$ (**4**), $[Cu(C_2O_4)(aind)_2]_n$ (**5**), $[Cu_2(C_2O_4)_2(bpzm)_2]_n\cdot(3.5H_2O)_n$ (**6**), $[Cu(C_2O_4)(ampy)(H_2O)]_n$ (**7**), $\{[Cu_2(\mu\text{-}C_2O_4)(aepy)_2][Cu(C_2O_4)_2(H_2O)_2]\}_n\cdot(2H_2O)_n$ (**8**) and $[Cu_4(\mu\text{-}C_2O_4)_3(aepy)_4(H_2O)_2]Cl_2$ (**9**) (pz = pyrazole, apz = 3(5)-aminopyrazole, mpz = 3(5)-methylpyrazole, ampz = 3(5)-amino-5(3)-methylpyrazole, aind = 7-azaindole, bpzm = bis(pyrazol-1-yl)methane, ampy = 2-aminomethylpyridine and aepy = 2-(2-pyridyl)ethylamine), are reported. On the basis of synthesis and structural characterization, the influence of neutral N-donor ligands on the control of the final complex structures and the role of weak intermolecular interactions in the creation of molecular architectures are discussed. Moreover, the magnetic properties of the complexes **1–9** have been investigated and discussed in the context of their structures.

‡ X-ray crystallographic data in CIF format, selected bond lengths and angles, short intra- and intermolecular contacts and PXRD patterns of compounds **1–9**. Crystallographic data for the structures reported in this article have been deposited in the Cambridge Crystallographic Data Center with CCDC 951616–951624 reference numbers for compounds **1–9**.

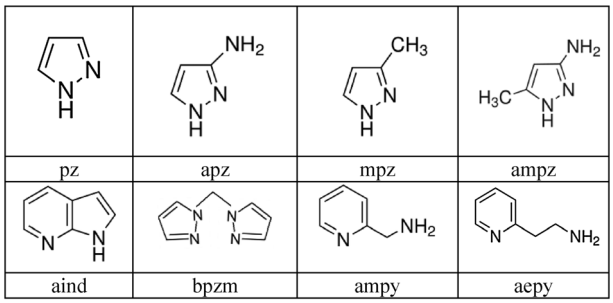

Scheme 2 Molecular structure of ligands used in this work.

Results and discussion

Preparation and general characterization

Synthesis and isolation of $[Cu(C_2O_4)(pz)]_n$ (**1**), $[Cu(C_2O_4)(apz)_2]_n\cdot(3H_2O)_n$ (**2**), $[Cu_2(\mu\text{-}C_2O_4)_2(H_2O)_2(ampz)_4]$ (**3**), $[Cu(C_2O_4)(mpz)_2]_n$ (**4**), $[Cu(C_2O_4)(aind)_2]_n$ (**5**), $[Cu_2(C_2O_4)_2(bpzm)_2]_n\cdot(3.5H_2O)_n$ (**6**), $[Cu(C_2O_4)(ampy)(H_2O)]_n$ (**7**), $\{[Cu_2(\mu\text{-}C_2O_4)(aepy)_2][Cu(C_2O_4)_2(H_2O)_2]\}_n\cdot(2H_2O)_n$ (**8**) and $[Cu_4(\mu\text{-}C_2O_4)_3(aepy)_4(H_2O)_2]Cl_2$ (**9**) were carried out through the self-assembly reactions of an aqueous solution of $(NH_4)_2C_2O_4$ with a methanolic solution of a copper salt and a suitable N-heterocyclic ligand (pz = pyrazole, apz = 3(5)-aminopyrazole, mpz = 3(5)-methylpyrazole, ampz = 3(5)-amino-5(3)-methylpyrazole, aind = 7-azaindole, bpzm = bis(pyrazol-1-yl)methane, ampy = 2-aminomethylpyridine and aepy = 2-(2-pyridyl)ethylamine), followed by solvent evaporation at room temperature. The reactions with pyrazole, 3(5)-aminopyrazole, 3(5)-methylpyrazole, 3(5)-amino-5(3)-methylpyrazole and 7-azaindole were carried out in a molar ratio of copper(II) chloride to ligand equal to 1 : 2. In the reactions with potentially chelating ligands, the metal-to-ligand ratio was equal to 1 : 1. Interestingly, the choice of copper(II) salt ($CuCl_2$ and $Cu(NO_3)_2$) turned out to be crucial only for complex formation with 2-(2-pyridyl)ethylamine. $Cu(NO_3)_2$ reacted with aepy and $(NH_4)_2C_2O_4$ to give $\{[Cu_2(\mu\text{-}C_2O_4)(aepy)_2][Cu(C_2O_4)_2(H_2O)_2]\}_n\cdot(2H_2O)_n$ (**8**), whereas the reaction of $CuCl_2$ with aepy and $(NH_4)_2C_2O_4$ yielded $[Cu_4(\mu\text{-}C_2O_4)_3(aepy)_4(H_2O)_2]Cl_2$ (**9**).

To confirm the phase purity of the synthesized complexes, the PXRD patterns of these compounds were recorded. As shown in Fig. S1–S9 (ESI†), all the XRPD patterns measured for the as-synthesized samples were in good agreement with the XRPD patterns simulated from the respective single-crystal X-ray data using the Mercury 2.4 program,[4] demonstrating

that the crystal structures are truly representative of the bulk materials.

The IR spectra of **1–9** show features attributable to each component of the complexes. In the high frequency region the IR spectra of **1–9** show strong absorptions assignable to N–H and O–H stretching vibrations (3480–3100 cm^{-1}). Coordination of the oxalate group was confirmed by absorptions in the region 1710–1630 and 1430–1270 cm^{-1} assigned to the asymmetric and symmetric stretching vibration of the $C_2O_4^{2-}$ group, respectively. These values agree well with those reported for the related oxalate complexes.[5] The characteristic bands assignable to ν(C=C) and ν(C=N) vibrations of coordinated N-heterocyclic ligands are observed in the range 1610–1500 cm^{-1}.[6]

Crystal structure analysis

The crystallographic data for **1–9** are summarized in Tables 1 and 2. The intra- and intermolecular contacts[7] detected in the structures **1–9** are collected in Table S1 (ESI†). The selected bond distances and angles of **1–9** are listed in Tables S2–S10 (ESI†).

Structure of $[Cu(C_2O_4)(pz)]_n$ (1)

Complex **1** crystallizes in the monoclinic space group $P2_1/c$. The asymmetric unit contains a metal ion, the pyrazole molecule and two halves of oxalate anions (Fig. 1a). The mid points of the C(4)–C(4A) and C(5)–C4(5C) bonds (symmetry codes as in Fig. 1) exist on the inversion centres (respectively, the special positions *a* and *c* of the $P2_1/c$ space group with the multiplicity 2). The pyrazole ligand is disordered over three positions with the 0.4 : 0.3 : 0.3 participation of partially occupied domains. The anisotropic displacement parameters (ADPs) of these disordered atoms show prolation and oblation effects, thus the atoms possessing most different ADPs (C(2) C(1A) N(2A) C(2A) C(1B) N(2B)) were restrained to be equal with effective standard deviation 0.01, and with the corresponding equivalent displacement parameters U_{eq} free to refine. One potential hydrogen bond donor (the N–H group) and one type of acceptor group (oxalate oxygen atoms) exist in the asymmetric unit of compound **1**, however the restraints imposed by the rigid polymer net disallow formation of a close contact between these groups. The lack of hydrogen bonding and relative rotational freedom about the Cu–N coordination bond favour the disorder of the neutral ligand of **1**. The two independent oxalate anions, situated at centers of inversion, adopt different coordination modes μ-oxalato-1κ^2O^1,O^2:2κ^2O^{1a},O^{2a} and μ_4-oxalato-1κ^2O^1,O^2:2κO^1:3κO^{1a},O^{2a}:4κO^{2a} (Fig. 1b) and connect the Cu centers into a two-dimensional net extending along the crystallographic plane (100) with Cu···Cu separations equal to 4.237(2), 5.546(2) and 5.553(2) Å (Fig. 1b and c). The pyrazole ligands alternatively extrude above and below the $[Cu(C_2O_4)]_n$ layer.

The centrosymmetric μ-oxalato-1κ^2O^1,O^2:2κ^2O^{1a},O^{2a} oxalate bridge (containing the O(3), O(4), and C(5) atoms) is attached to the copper centers with two short Cu–O bond distances of 1.9850(18) and 1.984(2) Å leading to an almost planar Cu–C_2O_4–Cu framework. The oxalate ligands incorporating O(1), O(2), and C(4) atoms coordinate to metal centers in two different modes, forming asymmetric chelate bis-bidentate linkage with a bond distance (2.3404(19) Å)

Table 1 Crystal data and structure refinement for **1–5** complexes incorporating monodentate ligands

	1	**2**	**3**	**4**	**5**
Empirical formula	$C_5H_4N_2O_4Cu$	$C_8H_{16}N_6O_7Cu$	$C_{10}H_{16}N_6O_5Cu$	$C_{10}H_{12}N_4O_4Cu$	$C_{16}H_{12}N_4O_4Cu$
Formula weight	219.64	371.81	363.83	315.78	387.8
Crystal system	Monoclinic	Triclinic	Orthorhombic	Monoclinic	Monoclinic
Space group	$P2_1/c$	$P\bar{1}$	*Pbcn*	$P2_1/n$	*C*2/*c*
Unit cell dimensions [Å, °]	a = 8.5694(6)	a = 9.0343(5)	a = 19.4230(5)	a = 7.2518(2)	a = 15.9790(10)
	b = 9.3227(4)	b = 9.2812(6)	b = 8.6184(2)	b = 8.3493(3)	b = 11.3100(8)
	c = 8.4631(9)	c = 10.1736(6)	c = 16.8313(5)	c = 20.4560(7)	c = 8.5968(5)
		α = 63.807(6)			
	β = 92.100(9)	β = 92.100(9)		β = 90.762(3)	β = 94.620(6)
		γ = 82.407(5)			
Volume [Å^3]	675.66(9)	737.05(8)	2817.48(13)	1238.45(7)	1548.59(17)
Z	4	2	8	4	4
Density (calculated) [Mg m^{-3}]	2.159	1.675	1.715	1.694	1.663
Absorption coefficient [mm^{-1}]	3.202	1.527	1.586	1.780	1.441
F(000)	436	382	1496	644	788
Crystal size [mm]	0.120 × 0.070 × 0.003	0.246 × 0.065 × 0.063	0.420 × 0.288 × 0.097	0.199 × 0.102 × 0.025	0.682 × 0.064 × 0.056
θ range for data collection [°]	3.98 to 29.27	3.36 to 25.05	3.38 to 25.05	3.72 to 25.04	3.60 to 25.04
Index ranges	$-11 \le h \le 11$	$-10 \le h \le 10$	$-23 \le h \le 23$	$-8 \le h \le 8$	$-18 \le h \le 18$
	$-12 \le k \le 12$	$-11 \le k \le 11$	$-10 \le k \le 10$	$-9 \le k \le 9$	$-13 \le k \le 11$
	$-10 \le l \le 10$	$-11 \le l \le 12$	$-20 \le l \le 20$	$-24 \le l \le 24$	$-10 \le l \le 10$
Reflections collected	5717	5566	21 909	11 694	4532
Independent reflections	1669 [R_{int} = 0.0400]	2604 [R_{int} = 0.0305]	2497 [R_{int} = 0.0443]	2187 (R_{int} = 0.0298)	1361 [R_{int} = 0.0338]
Completeness to 2theta [%]	99.7	99.8	99.8	99.8	99.7
Max. and min. transmission	1.000 and 0.715	1.000 and 0.878	1.000 and 0.749	1.000 and 0.811	1.00 and 0.785
Data/restraints/parameters	1669/36/181	2604/0/199	2497/0/201	2187/0/174	1361/0/114
Goodness-of-fit on F^2	1.020	1.056	1.036	1.067	1.057
Final R indices [$I > 2\sigma(I)$]	R_1 = 0.0363	R_1 = 0.0325	R_1 = 0.0329	R_1 = 0.0265	R_1 = 0.0287
	wR_2 = 0.0660	wR_2 = 0.0695	wR_2 = 0.0858	wR_2 = 0.0700	wR_2 = 0.0708
R indices (all data)	R_1 = 0.0619	R_1 = 0.0404	R_1 = 0.0401	R_1 = 0.0316	R_1 = 0.0337
	wR_2 = 0.0714	wR_2 = 0.0725	wR_2 = 0.894	wR_2 = 0.0723	wR_2 = 0.0724
Largest diff. peak and hole [e Å^{-3}]	0.529 and −0.593	0.298 and −0.267	0.326 and −0.316	0.306 and −0.260	0.301 and −0.227

Table 2 Crystal data and structure refinement for **6–9** complexes incorporating bidentate ligands

	6	7	8	9
Empirical formula	$C_{36}H_{48}N_{16}O_{23}Cu_4$	$C_8H_{10}N_2O_5Cu$	$C_{20}H_{28}N_4O_{16}Cu_3$	$C_{34}H_{44}N_8O_{14}Cl_2Cu_4$
Formula weight	1327.06	277.72	771.08	1113.83
Crystal system	Triclinic	Orthorhombic	Triclinic	Monoclinic
Space group	$P\bar{1}$	*Pbca*	$P\bar{1}$	$P2_1/c$
Unit cell dimensions [Å, °]	a = 9.1374(6)	a = 7.1301(3)	a = 7.6832(5)	a = 12.1604(6)
	b = 11.7993(7)	b = 12.8192(5)	b = 8.8480(6)	b = 7.1869(4)
	c = 12.2790(6)	c = 21.3279(7)	c = 10.4914(7)	c = 23.4200(15)
	α = 87.214(4)		α = 98.405(6)	
	β = 85.536(5)		β = 90.733(5)	β = 93.407(5)
	γ = 75.414(5)		γ = 101.710(6)	
Volume [Å^3]	1276.73(13)	1949.42(13)	690.21(8)	2043.2(2)
Z	1	8	1	2
Density (calculated) [Mg m^{-3}]	1.726	1.893	1.855	1.810
Absorption coefficient [mm^{-1}]	1.741	2.249	2.374	2.262
F(000)	676	1128	391	1132
Crystal size [mm]	0.581 × 0.234 × 0.233	0.254 × 0.206 × 0.01	0.189× 0.118 × 0.04	0.254 × 0.206 × 0.003
θ range for data collection [°]	3.57 to 25.05	3.32 to 25.00	3.42 to 25.05	3.29 to 25.04
Index ranges	$-10 \le h \le 10$	$-8 \le h \le 8$	$-9 \le h \le 9$	$-14 \le h \le 14$
	$-13 \le k \le 14$	$-15 \le k \le 15$	$-10 \le k \le 10$	$-8 \le k \le 7$
	$-14 \le l \le 14$	$-25 \le l \le 25$	$-12 \le l \le 11$	$-27 \le l \le 23$
Reflections collected	13 783	19 304	5160	11 007
Independent reflections	4504 (R_{int} = 0. 0340)	1718 [R_{int} = 0.0531]	2441 (R_{int} = 0.0284)	3615 [R_{int} = 0.0417]
Completeness to 2theta [%]	99.5	99.9	99.7	99.9
Max. and min. transmission	1.000 and 0.382	1.000 and 0.567	1.000 and 0.701	1.00 and 0.891
Data/restraints/parameters	4504/0/358	1718/0/145	2441/0/196	3615/0/299
Goodness-of-fit on F^2	1.171	1.087	1.053	1.180
Final R indices [$I > 2\sigma(I)$]	R_1 = 0.0397	R_1 = 0.0261	R_1 = 0.0315	R_1 = 0.0397
	wR_2 = 0.1212	wR_2 = 0.0717	wR_2 = 0.0722	wR_2 = 0.1060
R indices (all data)	R_1 = 0.0547	R_1 = 0.0320	R_1 = 0.0381	R_1 = 0.0487
	wR_2 = 0.1426	wR_2 = 0.0735	wR_2 = 0.0761	wR_2 = 0.1090
Largest diff. peak and hole [e Å^3]	0.529 and −0.597	0.296 and −0.408	0.320 and −0.353	0.766 and −0.449

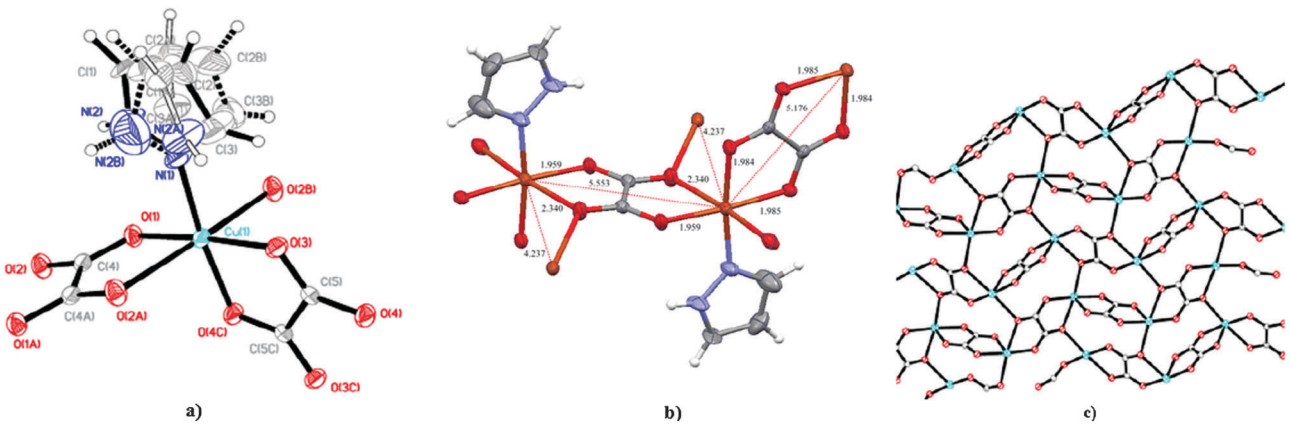

Fig. 1 (a) The perspective drawing of the coordination entity of compound **1**, the symmetry generated atoms are indicated by A, B and C letters (symmetry codes $-x, -y, -z$; $-x, y + 0.5, -z + 0.5$ and $-x, -y + 1, -z$); (b) the fragment showing two different coordination modes of oxalate ligands with Cu–O bond lengths and Cu···Cu separations; (c) the part of the 2D coordination network, the ligand molecules not involved into formation of the net were omitted.

significantly longer than the other one (1.9589(18) Å) and in a monodentate way with bond lengths of 2.4984(18) Å. As a result, the coordination environment around each Cu(II) ion is a tetragonally elongated octahedron with the equatorial plane defined by three oxalate oxygen atoms O(1), O(3) and O(4)^i [(i) $-x, -y + 1, -z$] and one pyrazole nitrogen atom. The axial coordination sites are occupied by the oxalate oxygen atoms with Cu–O bond lengths of 2.3404(19) and 2.4984(18) Å, which are significantly longer than the equatorial ones (Table S2, ESI†).

The Cu–O_{ox} distances and O–Cu–O bond angles of **1** fall within the range typical for oxalate bridged Cu(II) complexes. The C(5)–C(5)^i [(i) $-x, -y + 1, -z$] and C(4)–C(4)^{ii} [(ii) $-x, -y, -z$] bond lengths are 1.525(5) and 1.551(6) Å, which correspond to a single bond. The C(4)–O(1) and C(5)–O(4) (whose oxygen atoms are engaged in both bidentate and monodentate bridges) are longer than C(4)–O(2) and C(5)–O(3), as expected from the polarisation of the charge density towards the metal-bonded oxygen atoms.[8]

To get better insight into the framework structure of **1**, topological analysis was carried out which revealed that the metal centres create the 7-c uninodal net (Fig. 1c), described by the $\{3^9;4^9;5^3\}$ Schläfli symbol and the [3.3.3.3.3.3.3.3.3.4.4.4.4.4.4.4.4.5.5(2).5(2)] extended point vertex symbol.[9] This means that the net is formed by alternating hexa- and tetra-functional oxalate ions (coordinating to four metal ions in two bidentate-chelating modes and two monodentate modes, and to two metal ions in two bidentate-chelating modes, Fig. 1c).

Structure of $[Cu(C_2O_4)(apz)_2]_n\cdot(3H_2O)_n$ (2)

The structure of **2** consists of $[Cu(C_2O_4)(apz)_2]$ and solvated water molecules. The $[Cu(C_2O_4)(apz)_2]$ units are linked by alternating amino nitrogen atoms of the apz ligand and oxygen atoms of the oxalate ion to give an infinite one-dimensional zig-zag chain propagating along the [010] direction (Fig. 2).

The Cu···Cu distances separated by 5-aminopyrazole and μ-oxalato-1κ^2O^1,O^2:2κO^{1a} ligands are 4.583(2) and 5.533(2) Å, respectively.

The coordination geometry around the Cu(II) ion can be described as a tetragonally elongated octahedron with the oxygen atom from the $C_2O_4^{2-}$ ion (Cu(1)–O(2)^i = 2.921(3) Å [(i): $-x$, $1-y$, $1-z$]) and the amino nitrogen atom of the apz ligand (Cu(1)–N(3)^{ii} = 2.445(2) Å [(ii): $-x$, $2-y$, $1-z$]) in the axial positions. The equatorial plane is constituted by two nitrogen atoms of pyrazole molecules (Cu(1)–N(1) = 2.004(2) Å, Cu(1)–N(4) = 1.977(2) Å) and two oxygen atoms of the oxalate ion (Cu(1)–O(1) = 1.9836(18) Å, Cu(1)–O(3) = 1.9551(18) Å). The two tri-functional bridging oxalate ions (coordinating to two metal ions in bidentate-chelating and monodentate modes, Fig. 2b) alternating in the polymeric chain with the two di-functional bridging pyrazole molecules (coordinating to two metal ions in monodentate mode, Fig. 2b) form the 1D coordination polymer possessing the double bridged copper ions.

The Cu(1)–O(2)^i [(i) $-x$, $1-y$, $1-z$] bond length exceeds the Cu–O$_{eq}$ ones by *ca.* 0.96 Å, and it is similar to that in $[Cu_2(BIBM)_2(C_2O_4)_2]\cdot4H_2O$ (BIBM = bis(2-imidazolyl)bis(methoxycarbonyl)methylmethane), where the oxalate groups also act in a monodentante–bidentate mode.[10] According to Hathaway's criterion the axial oxalate oxygen atom is in the borderline to be considered as semicoordinated.[11] The pyrazole rings are close to planarity (a maximum deviation of 0.0030(16) Å exists for the N(1) atom in one of the planes and 0.0013(16) Å for the N(4) atom in the second plane) and they are inclined at 74.52(13)°. The oxalate group is approximately planar with deviations up to 0.064(4) Å from the least-squares plane and makes a dihedral angle of 7.71(15)° with the equatorial plane of the Cu(1) center formed by N(1), N(4), O(1) and O(3) atoms. The C(7)–C(8) bond distance of 1.543(4) Å reflects carbon–carbon single bond character. The C–O bond lengths satisfy the trend C–O$_{coord}$ > C–O$_{semicoord}$ > C–O$_{uncoord}$, as expected from the polarization of the charge density toward the metal-bonded oxygen atoms. The presence of multiple N–H (complex molecule) and O–H (water molecules) hydrogen bond donors in different environments leads to the complex scheme of intramolecular interactions. The unitary basic graph set is composed of DDDDC(11)[R_2^2(14)]DDDDs(5)S(8)DD basic motifs, respectively for bonds listed in Table S1 (ESI†). These interactions expand the molecules to the three-dimensional supramolecular network.

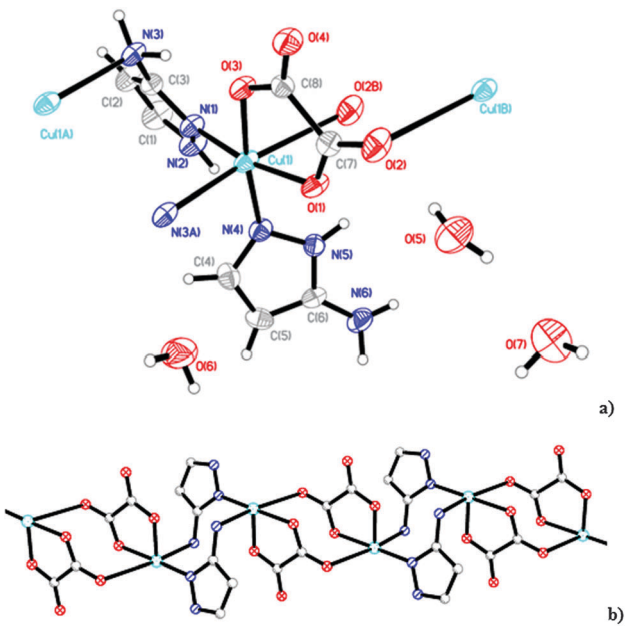

Fig. 2 (a) The perspective drawing of the coordination entity of compound **2**, the symmetry generated atoms are indicated by A and B letters (symmetry codes $-x$, $-y+2$, $-z+1$ and $-x$, $-y+1$, $-z+1$ respectively); (b) the part of the 1D coordination network, the ligand molecules not involved in formation of the chain and hydrogen atoms were omitted.

Structure of $[Cu_2(\mu\text{-}C_2O_4)_2(H_2O)_2(ampz)_4]$ (3)

The structure **3** is built up of centrosymmetric dimeric $[Cu_2(\mu\text{-}C_2O_4)_2(H_2O)_2(ampz)_4]$ entities which are linked through hydrogen bonds involving water molecules and 5-amino-3-methylpyrazole/oxalato moieties. A view of dimeric unit $[Cu_2(\mu\text{-}C_2O_4)_2(H_2O)_2(ampz)_4]$ is depicted in Fig. 3, and its relevant bond distances

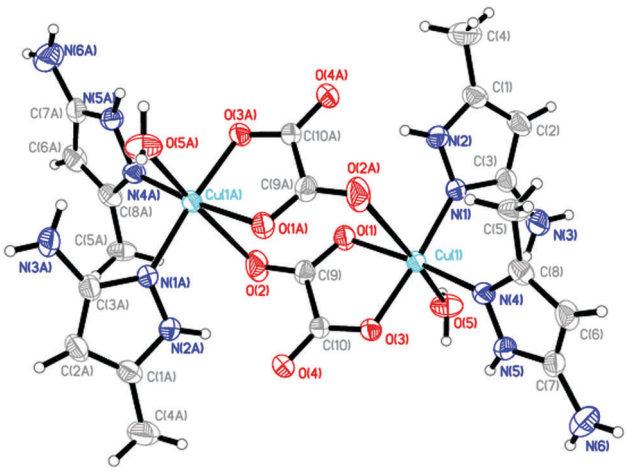

Fig. 3 The perspective drawing of the dimeric coordination unit of compound **3**, the symmetry generated atoms are indicated by letter A (symmetry code $-x+1$, $-y$, $-z$).

and angles are reported in Table S4 (ESI†). The dinuclear units are constructed *via* oxalate ions analogously to linkage observed in compound **2**, *i.e.* the two tri-functional bridging oxalate ions (coordinating to two metal cations in bidentate-chelating and monodentate modes, Fig. 3) join two copper ions.

The dinuclear complex results from the pairing of two mononuclear units $[Cu(C_2O_4)(H_2O)(ampz)_2]$ related by a crystallographic center of inversion. Two centrosymmetrically related copper(II) centers are bridged by two oxalate groups which act in a monodentante–bidentate mode. The resulting intra-dinuclear Cu···Cu separation of 5.424(2) Å falls in the range reported for the related Cu(II) species.[12] Taking the semi-coordinated oxygen atom into consideration, the coordination about the copper(II) ions can be described as an elongated octahedron. The equatorial plane is comprised of two oxygen atoms belonging to an oxalate group and two nitrogen atoms from two ampz molecules. The four equatorial atoms are nearly coplanar within ±0.002(12) Å, and the copper atom is displaced by 0.100(2) Å in the least-squares plane towards the ligand in the apical site. The pyrazole mean planes make dihedral angles of 56.26(10)° and 52.12(10)° with the equatorial plane, and the dihedral angle between the two pyrazole rings is 66.64(13)°. The oxalate group is bound to the copper atom in an approximately symmetrical manner with the Cu(1)–O(1) and Cu(1)–O(3) bond lengths 1.962(2) and 1.968(2) Å, respectively. It is approximately planar with deviations up to 0.0383(3) Å from the least-squares plane and makes a dihedral angle of 4.28(15)° with the equatorial plane of the Cu(1) atom. The axial coordination sites are occupied by oxygen atoms belonging to the water molecule and the oxalate group, with Cu–O bond lengths of 2.404(2) and 2.915(3) Å, which are significantly longer than the equatorial ones. Both uncoordinated and semicoordinated oxygen atoms are also affected by H-bonding. The dimer is internally linked by four N–H···O hydrogen bonds forming two $N_1R_2^2(14)$ motifs and two pairs of $N_2R_1^2(5)R_2^2(14)$ motifs. The dinculear units are assembled *via* the intermolecular N–H···O, O–H···O and O–H···N hydrogen bonds (Table S1, ESI†) to the three-dimensional supramolecular network. These bond motifs form the $C(7)R_2^2(10)R_2^2(10)C(7)$ unitary basic graph set. Two of the above mentioned interactions (N–H···O and O–H···N) create a double hydrogen bond. Additionally in the structure can be found several C–H···O short contacts (Table S1, ESI†), which can be considered as weak hydrogen bonds. These interactions provide an additional stabilization to the supramolecular architecture.

Structure of $[Cu(C_2O_4)(mpz)_2]_n$ (4)

The crystal structure of **4** is built of $[Cu(mpz)_2]^{2+}$ units joined sequentially by μ-oxalato-1κ^2O^1,O^2:2κO^{1a} ligands to zig-zag chains parallel to the [010] direction with Cu···Cu intrachain separations of 6.300(2) Å (Fig. 4). Each tri-functional bridging oxalate ion coordinates to two metal ions (in bidentate-chelating and monodentate modes, Fig. 4b) forming the 1D coordination polymer, with in-chain linkage same as in compound **7**. Each copper(II) is five-coordinated by two oxygen atoms (Cu(1)–O(1), 1.9345(16) Å and Cu(1)–O(3), 1.9651(15) Å) from the oxalate ligand and two nitrogen atoms (Cu(1)–N(1), 1.9708(19) Å and Cu(1)–N(2), 1.9766(19) Å) of mpz ligands to form the basal plane and the coordination sphere is completed by an apical oxygen atom from another oxalate with a longer bond (Cu(1)–O(4), 2.4157(17) Å) (Table S5, ESI†).

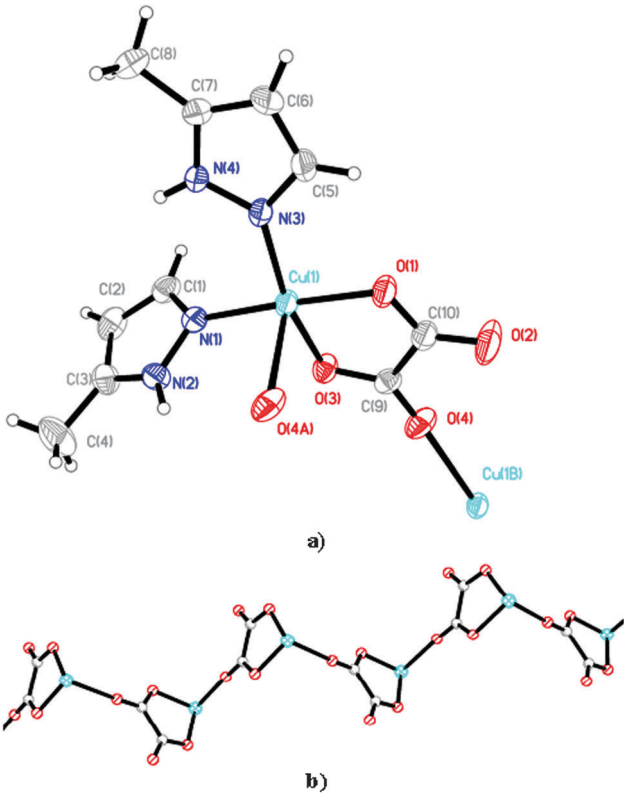

Fig. 4 (a) The perspective drawing of the coordination entity of compound **4**, the symmetry generated atoms are indicated by A and B letters (symmetry codes $-x-0.5, y-0.5, -z+0.5$ and $-x-0.5, y+0.5, -z+0.5$ respectively); (b) the part of the 1D coordination network, the ligand molecules not involved in formation of the chain were omitted.

The coordination geometry at the copper center can be described as a distorted square pyramid with a parameter τ equal to 0.22(1).[13] The pyrazole rings are close to planarity (a maximum deviation of 0.0032(14) Å exists for the N(1) atom in one of the planes and 0.0024(18) for the C(5) atom in the second plane) and are inclined at 61.50(8)°. The oxalate group is approximately planar with deviations up to 0.024(3) Å from the least-squares plane and makes a dihedral angle of 5.83(12)° with the equatorial plane of the Cu(1) center formed by N(1), N(3), O(1) and O(3) atoms. The C(9)–C(10) bond distance of 1.554(3) Å reflects carbon–carbon single bond character. The C–O bond lengths satisfy the trend $C–O_{coord} > C–O_{semicoord} > C–O_{uncoord}$, as expected from the polarization of the charge density toward the metal-bonded oxygen atoms.

The chains of **4** are internally linked by N–H···O hydrogen bonds. Such type of bond also interlinks the neighboring chains to the C(5) unitary graph motif of the lowest degree and the $C(7+2n)$ motif of higher degrees (where $n \subset \aleph_0$). These interactions form a layer extending along the crystallographic (001) plane. In the structure of **4** also exists two types of C–H···O short contacts (one inter-chain and one intra-chain, Table S1, ESI†), which can be classified as weak hydrogen bonds.

Structure of $[Cu(C_2O_4)(aind)_2]_n$ (5)

The structure **5** consists of *cis*-$[Cu(aind)_2]^{2+}$ units bridged sequentially by bis-bidentate, oxalate ligands to form a zig-zag polymeric chain parallel to [001] (Fig. 5). The mid point of the C(8)–C(8A) bond (symmetry code as in Fig. 5) exists on the inversion centre (the special positions *b* of the *C*2/*c* space group with the multiplicity 4). Each tetra-functional bridging oxalate ion coordinates to two metal ions (each in bidentate-chelating mode, Fig. 5b) forming the 1D coordination polymer, with in-chain linkage the same as in compounds **6** and **8**. The Cu···Cu separation across the bridging oxalate group is 5.541(2) Å, typical of bis-bidentate oxalate-bridged copper(II) complexes, namely 5.411(2) Å in $[Cu_2(\mu\text{-}C_2O_4)_2(ampy)_3]_n$[14] and 5.419(2) and 5.544(2) Å in $[Cu_3(\mu\text{-}C_2O_4)_3(\mu\text{-}4,4'\text{-bipy})_2(4,4\text{-bipy})]_n$.[15] The Cu(II) centres, placed on a crystallographic 2-fold axis (the special position *e* of the *C*2/*c* space group with the multiplicity 4), are coordinated to four oxygen atoms from two symmetry related bridging oxalate ligands and the pyridine-type nitrogen atoms of two symmetry related, *cis*-arranged 7-azaindole ligands. The metal coordination geometry is well described as Jahn–Teller distorted octahedral with four short bonds formed by the imine nitrogen atoms, from two crystallographically related aind molecules (Cu(1)–N(1) 2.0254(18) Å) and two oxygen atoms from two asymmetrically ligated oxalate ions (Cu(1)–O(1) 1.9936(14) Å). The axial coordination sites are occupied by the two remaining oxalate oxygen atoms, with the C–O bond length (2.3053(15) Å) that is significantly longer than the equatorial one (Table S6, ESI†). The difference between the Cu–O_{ax} and Cu–O_{eq} distances (0.31(1) Å) correlates with those observed in the related $[Cu_2(\mu\text{-}C_2O_4)_2(ampy)_3]_n$[14] and $[Cu_3(\mu\text{-}C_2O_4)_3(\mu\text{-}4,4'\text{-bipy})_2(4,4\text{-bipy})]_n$.[15]

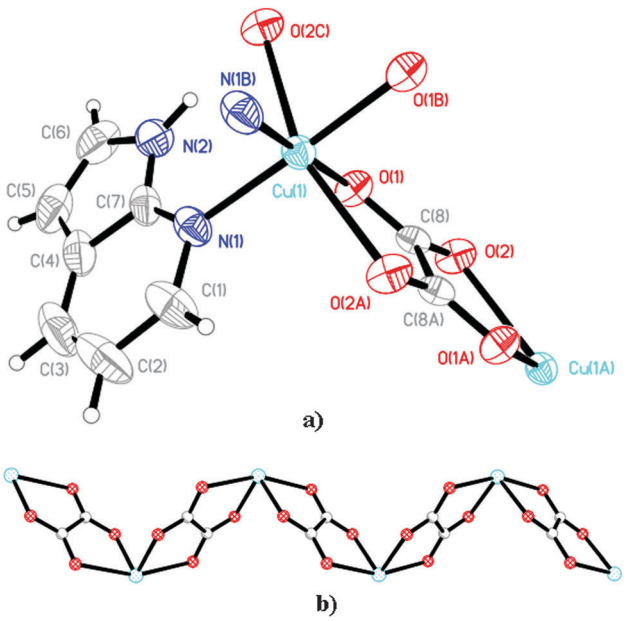

Fig. 5 (a) The perspective drawing of the coordination entity of compound **5**, the symmetry generated atoms are indicated by A, B and C letters (symmetry codes $-x, -y+1, -z+1$; $-x, y, -z+1/2$ and $x, -y+1, z-1/2$ respectively); (b) part of the 1D coordination network, the ligand molecules not involved in formation of the chain were omitted.

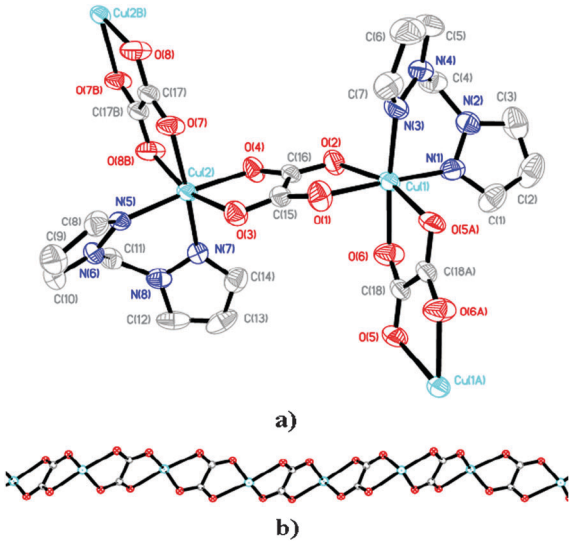

Fig. 6 (a) The perspective drawing of the coordination entity of compound **6**, the symmetry generated atoms are indicated by A and B letters (symmetry codes $-x, -y+1, -z+1$ and $-x+1, -y, -z$ respectively), the hydrogen atoms and water molecules were omitted for clarity; (b) the part of the 1D coordination network, the ligand molecules not involved in formation of the chain were omitted.

The oxalate and aind ligands form dihedral angles of 79.29(3)° and 68.7(3)°, respectively, with the equatorial coordination plane.

Similarly to **4**, the chains of **5** are internally linked by N–H···O hydrogen bonds, but, in opposition to **4**, there are no hydrogen bonds between the chains (even the weak ones).

Structure of $[Cu_2(C_2O_4)_2(bpzm)_2]_n \cdot (3.5H_2O)_n$ (6)

The asymmetric unit of **6** (Fig. 6a) consists of non-centrosymmetric dinuclear units $[Cu_2(C_2O_4)_2(bpzm)_2]$ and crystallization water molecules. The dinuclear $[Cu_2(C_2O_4)_2(bpzm)_2]$ entities are further linked into a zig-zag polymeric chain parallel to [1−1−1] (Fig. 6b). Each tetra-functional bridging oxalate ion coordinates to two metal ions (each in a bidentate-chelating mode, Fig. 6b) forming the 1D coordination polymer, with in-chain linkage the same as in compounds **5** and **8**. The coordination environment around ions Cu(1) and Cu(2) is a tetragonally elongated octahedron with four short bonds formed by nitrogen atoms of the bpzm ligand and two oxygen atoms from oxalate ions. The axial coordination sites are occupied by the two remaining oxalate oxygen atoms, with C–O bond lengths longer than the equatorial ones (Table S7, ESI†). The Cu(1)···Cu(1) and Cu(1)···Cu(2) separations through the bidentate oxalate bridges are 5.507(4) and 5.464(4) Å, respectively.

Structure of $[Cu(C_2O_4)(ampy)(H_2O)]_n$ (7)

In structure **7**, the $[Cu(C_2O_4)(ampy)(H_2O)]$ molecules are associated through a Cu–O semi-coordination bond of 2.830(2) Å to form zig-zag chains running along the [100] direction with an intra-chain Cu···Cu separation of 5.085(2) Å (Fig. 7). Each tri-functional bridging oxalate ion coordinates to two metal ions (in bidentate-chelating and monodentate modes, Fig. 7b) forming the 1D coordination polymer, with in-chain linkage the same as in

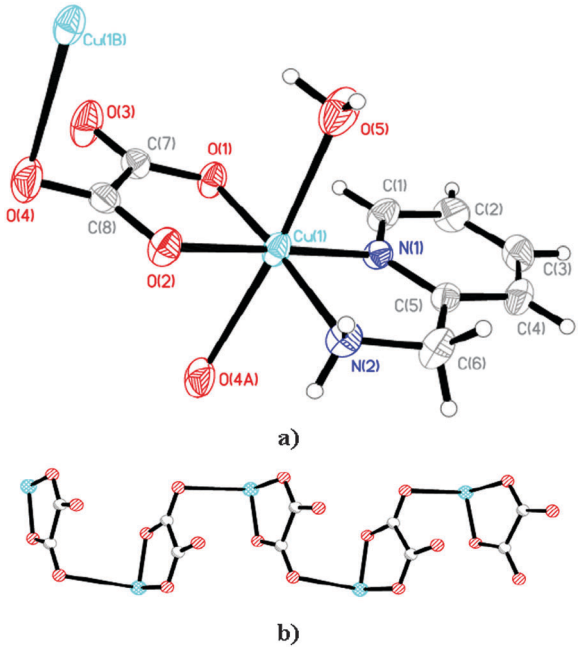

Fig. 7 (a) The perspective drawing of the coordination entity of compound **7**, the symmetry generated atoms are indicated by A and B letters (symmetry codes $x + 0.5, y, -z + 0.5$ and $x - 0.5, y, -z + 0.5$ respectively); (b) the part of the 1D coordination network, the ligand molecules not involved in formation of the chain were omitted.

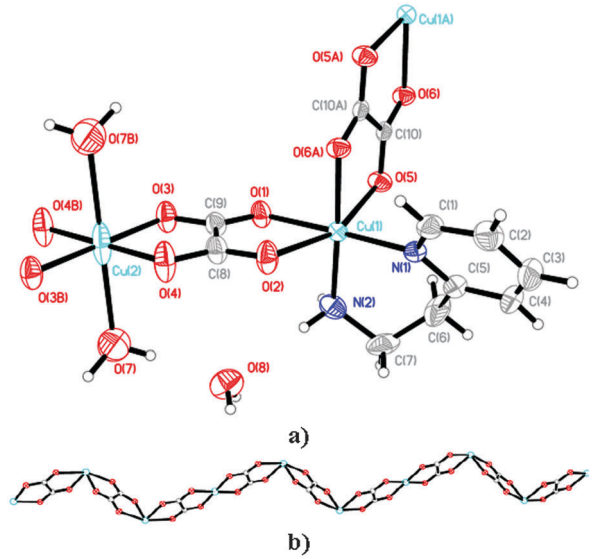

Fig. 8 (a) The perspective drawing of the coordination entity of compound **8**, the symmetry generated atoms are indicated by A and B letters (symmetry codes $-x + 1, -y + 1, -z + 1$ and $-x, -y, -z$ respectively); (b) the part of the 1D coordination network, the ligand molecules not involved in formation of the chain were omitted.

compound **4**. These chains are internally stabilized by two hydrogen bonds, one N–H···O and one O–H···O, both forming C(4) motifs of a basic unitary graph set composed of molecules considered as separated ones (Table S1, ESI†). Taking the semi-coordinated oxygen atom into consideration, the copper(II) ion of **7** displays a tetragonally elongated octahedron. The equatorial coordination positions involve two oxalate oxygen atoms and two nitrogen atoms of ampy coordinated to the central ion in a chelating way. The axial coordination sites are occupied by the oxalate and water oxygen atoms with Cu–O bond lengths of 2.830(2) and 2.487(2) Å which are significantly longer than the equatorial ones 1.9438(18) and 1.9549(18) Å (Table S8, ESI†).

The above mentioned chains are assembled *via* N–H···O and O–H···O bonds (both creating C(6) motifs of the basic unitary graph set) to the two dimensional supramolecular network extending along the crystallographic (001) plane. One C–H···O short contact (Table S1, ESI†), which can be considered as a weak hydrogen bond, provides additional linkage between the chains of the supramolecular network. Additionally the molecules of **7** contain the intramolecular C–H···O interactions (Table S1, ESI†) which can be classified as weak intramolecular hydrogen bonds.

Structure of $\{[Cu_2(\mu\text{-}C_2O_4)(aepy)_2][Cu(C_2O_4)_2(H_2O)_2]\}_n \cdot (2H_2O)_n$ (8)

The crystal structure of **8** is comprised of zig-zag chains built of the centrosymmetric binuclear $[Cu_2(\mu\text{-}C_2O_4)(aepy)_2]^{2+}$ cations joined sequentially by $[Cu(C_2O_4)_2(H_2O)_2]^{2-}$ anions and solvated water molecules (Fig. 8). Each tetra-functional bridging oxalate ion coordinates to two metal ions (each in bidentate-chelating mode, Fig. 8b) forming the 1D coordination polymer, with in-chain linkage the same as in compounds **5** and **6**. There are two different copper centers in crystal structure **8**, Cu(1) in the cationic unit and Cu(2) in the anionic unit. The coordination environment around both Cu(1) and Cu(2) ions is a tetragonally elongated octahedron. The equatorial coordination positions of Cu(1) involve two oxalate oxygen atoms O(1) and $O(10)^i$ [(i) $-x + 1, -y + 1, -z + 1$] and two nitrogen atoms of the chelating aepy ligand. The axial coordination sites are occupied by the oxalate oxygen atoms with the Cu–O bond length greater than the Cu–O_{eq} by *ca.* 0.3 Å (Table S9, ESI†). The Cu(2) atom occupies a special position (the special position *a* of the $P\bar{1}$ space group with the multiplicity 1), and its basal plane of Cu(2) ions is defined by four oxygen atoms from two crystallographically related bidentate oxalate ligands with almost equal Cu–O bond distances 1.946(2) and 1.9556(18) Å. The mid point of the C(10)–C(10A) exist on the inversion centre (the special position *h* of the $P\bar{1}$ space group with the multiplicity 1). The coordination sphere of Cu(2) is completed by two water molecules occupying axial positions and symmetrically related. As expected the Cu–O_{water} bond length (2.531(3) Å) is considerably greater than the Cu–O_{eq}. The Cu(1)···Cu(1) and Cu(1)···Cu(2) separations through the bidentate oxalate bridges are 5.576(2) and 5.365(2) Å, respectively. Two crystallographically related oxalate ligands form dihedral angles of 3.3(3)° with the equatorial coordination plane of Cu(2), whereas the dihedral angles between the oxalate ions and the equatorial plane of the central ion Cu(1) are equal to 88.5(3) and 87.6(3)°.

The polymeric chains and the outer coordination sphere water molecules of compound **8** are linked by N–H···O and O–H···O to the three dimensional supramolecular network, and the basic unitary graph set consists of $DDR_2^2(4)[C(6)]DD$ motifs, respectively, for interactions listed in Table S1 (ESI†).

One water molecule is involved in the O–H···π hydrogen bond formed between the O7–H7OA donor and the pyridine ring acceptor (containing N1/C1/C2/C3/C4/C5 atoms), with a D···A distance of 3.351(2) Å, a H···D distance of 2.388 Å and a D–H···A angle of 168.6°. The supramolecular network is cross-linked by two different types of C–H···O weak hydrogen bonds and the polymer chains are additionally stabilized by one C–H···O weak intramolecular hydrogen bond.

Structure of $[Cu_4(\mu\text{-}C_2O_4)_3(aepy)(H_2O)_2]Cl_2$ (9)

The structure of **9** consists of tetranuclear complexes $[Cu_4(\mu\text{-}C_2O_4)_3(aepy)_4]^{2+}$ and chloride ions. The tetranuclear complex $[Cu_4(\mu\text{-}C_2O_4)_3(aepy)_4(H_2O)_2]^{2+}$ (Fig. 9) results from the pairing of two dinuclear units $[Cu_2(\mu\text{-}C_2O_4)_{1.5}(aepy)_2(H_2O)]^{+}$ related by a crystallographic center of inversion located in the middle of the C–C bond of this central μ-oxalato bridge.

The tetramers are constructed *via* oxalate ions analogously to linkage observed in compounds **5**, **6** and **8**, *i.e.* the three tetra-functional bridging oxalate ions (coordinating to two metal ions in bidentate-chelating mode), Fig. 9, join four copper ions. The two Cu atoms of the tetramer are coordinated by two oxalate and aepy ligands, which build up an elongated octahedral surrounding around Cu(1). Both bis-chelating oxalato bridges are asymmetrically coordinated to the Cu(1) atom with one Cu–O bond distance [2.363(3) and 2.273(3) Å for Cu(1)–O(3) and Cu(1)–O(7), respectively] significantly longer than the other one [2.088(3) and 1.0986(3) Å for Cu(1)–O(1) and Cu(1)–O(6), respectively]. The oxygen atoms O(1) and O(6) involved in the short bond distances and nitrogen atoms N(1) and N(2) of the aepy ligand define the equatorial plane of the octahedron around Cu(1). The apical positions are filled by the O(3) and O(7) atoms involved in the longest bond distances. The dihedral angle between the two bridging oxalato ligands around the Cu(1) is 88.6(4)°, and the oxalato bridges form dihedral angles of 87.8(4) and 75.1(4)° with the best equatorial mean plane of the Cu(1) center (Table S10, ESI†). The two outer Cu atoms have a square-pyramidal environment, with two oxygen atoms of the oxalate bridge and two nitrogen atoms of aepy occupying the base of the pyramid. The axial co-ordination site is occupied by the oxygen atom of the water molecule.

In contrast to Cu(1), the coordination of the bridging oxalato ligands to Cu(2) is almost symmetric, with two very short Cu–O bond distances (1.988(3) and 1.971(3) Å for Cu(2)–O(2) and Cu(2)–O(4), respectively). The dihedral angle between the bridging oxalato ligand and the best equatorial mean plane of Cu(2) is 5.0(4)°. The metal–metal distances across the two oxalato bridges are 5.434(3) Å, [Cu(1)···Cu(2)] and 5.525(3) Å [Cu(1)···Cu(1a)]. In the dimer, the oxalato bridge is asymmetrically coordinated to the copper atom which exhibits a tetragonally elongated CuO4N2 environment, whereas it is linked to the five-coordinated copper atom by means of two short Cu–O distances.

The tetranuclear complex cation is internally linked to the four C–H···O weak hydrogen bonds (two bonds in each asymmetric unit). The N–H···O hydrogen bonds links the cation to the supramolecular rings $(R_2^2(20)R_2^2(24)$ unitary graph motifs) and the N/O–H···Cl hydrogen bonds form the finite D motifs of the first level graph. At the higher levels all these interactions assemble the cations and anions to the two dimensional layer extending along the crystallographic (102) plane. These layers are linked by the C–H···O/Cl intermolecular hydrogen bonds to the three dimensional supramolecular network.

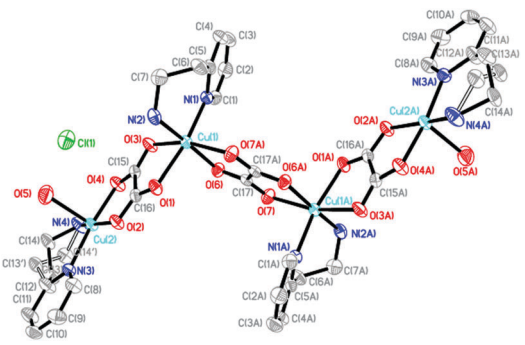

Fig. 9 The perspective drawing of the tetranuclear coordination cation and the asymmetric unit anion of compound **9**, the symmetry generated atoms are indicated by letter A (symmetry code $-x, -y + 1, -z + 1$), the hydrogen atoms were omitted for clarity, the bonds of disordered domains are drawn as hollow lines.

Effect of the N-donor ligand on the structures

Through varying the auxiliary N-donor ligands under similar synthetic conditions nine new copper(II) oxalate compounds with different structures were successfully obtained. Depending on the features of the N-donor ligands (substituents and coordination groups, conformations, and flexibility), the resultant compounds differ in dimensionality, metal coordination sphere or oxalate coordination modes. The two dimensional network is formed only in the case of the compound containing only one monofunctional organic N-donor ligand, *i.e.* compound **1**. In other studied compounds, two or three N-donor ligands exist on the inner coordination sphere, or one such ligand acts in the chelating mode. Thus in only **1**, five more coordination sites are available (instead of four less sites existing in compounds **2–9**) after coordination of the organic ligand, and 2D structure is achieved by a very rare μ_4-oxalato-$1\kappa^2O^1,O^2:2\kappa O^1:3\kappa O^{1a},O^{2a}:4\kappa O^{2a}$ coordination mode of oxalate ions. The pyrazole ligands alternatively extrude above and below the $[Cu(C_2O_4)]_n$ layer.

The introduction of additional substituents into the pyrazole ring (3-amino in apz, methyl in mpz, amino and methyl in ampz) or existence of an extended π-conjugated system (7-azaindole) increases the complexation properties of N-donor ligands, consequently leading to formation of more stable $M:L_2$, $M:L_3$, and $M:L_{chelating}$ coordination compounds, and finally results in the low dimensional networks, 1D for $[Cu(C_2O_4)(apz)_2]_n{\cdot}3nH_2O$ (**2**) $[Cu(C_2O_4)(mpz)_2]_n$ (**4**) and $[Cu(C_2O_4)(aind)_2]_n$ (**5**), and 0D dimeric structure for $[Cu_2(\mu\text{-}ox)_2(H_2O)_2(ampz)_4]$ (**3**). The presence of the amino group in apz plays a key role in the formation of the final structure of **2** being an infinite one-dimensional zig-zag chain with

$[Cu(C_2O_4)(apz)_2]$ units linked by alternating amino nitrogen atoms of the apz ligand and oxygen atoms of oxalate ions. Simultaneous existence of both amino and methyl groups in the ampz ligand results in formation of a 0D dimeric structure of **3**, stabilized by extensive hydrogen-bonding interactions. The water molecules are built up to the inner coordination sphere of compounds in which exist a residual space around the metal after formation of the coordination bonds with the N-donor and oxalate ligands, and in which, both the steric hindrance of the N-donor and oxalate ligands and the absence of the respective species in the reaction environments disallow formation of subsequent Cu–N and Cu–$O_{oxalate}$ bonds.

The substituents of the pyrazole ring also influence the coordination modes of oxalate anions. The structures **2**, **3** and **4** display a rather unusual mono/bidentate coordination mode (μ-oxalato-$1\kappa^2O^1,O^2{:}2\kappa O^{1a}$) of oxalate ligands, whereas the metal centers of **5** are typically bridged by bis-bidentate oxalate ions (μ-oxalato-$1\kappa^2O^1,O^2{:}2\kappa^2O^{1a},O^{2a}$). The same oxalate coordination mode was confirmed for $[Cu_2(C_2O_4)_2(bpzm)_2]_n{\cdot}(3.5H_2O)_n$ (**6**). In contrast to **5**, however, the zig-zag polymeric chain of **6** is built of dinuclear units. The structural difference of compounds **7** or **8** and **9**, noticeable in the metal coordination environments and oxalate coordination modes, is mainly attributed to the effect of the spacer length and flexibility of the N-donor ligand. Compared with the ampy ligand, the aepy ligand has an additional $-CH_2-$ group. The role of coordinated and lattice water molecules as well as extensive hydrogen-bonding interactions is also important in these structures.

Thermal analysis

The thermal stability of compounds **1–9** was measured by TGA on polycrystalline samples in an air atmosphere with a heating rate of 20 °C min^{-1}. The TG analyses of **2**, **6**, **7** and **8** show the first weight loss of 14.316% (50–113 °C, calcd 14.54%) for **2**, 9.87% (80–148 °C, calcd 9.52%) for **6**, 6.5% (165–209 °C, calcd 6.49%) for **7** and 9.43% (55–229.1 °C, calcd 9.35%) for **8**, corresponding to the loss of coordinated or lattice water molecules per formula unit (Fig. S10, ESI†). After that, the weight loss occurs upon heating including three steps for **7** and **8** and four for **2** and **8**. The weight losses in the range of 130–290 °C for **2**, 205–289 °C for **7** and 202–298 °C for **8** correspond to the removal of the corresponding organic components, 44.91% (calcd 44,70%) for **2**, 37.5% (calcd 38.94%) for **7** and 46.15% (calcd 47.53%) for **8**. The anhydrous framework of **6** starts to decompose beyond 165.5 °C in a series of complicated overlapped weight losses. The final mass remnant is of 25.1% for **2**, 10.5% for **6**, 25.4% for **7** and 28.0% for **8** of the total sample. The complex **1** remains intact until heating to 229.3 °C, and then suffers two consecutive weight losses that end at 430 °C. The *pz* molecules are lost in the first step followed by degradation. Further heating to 800 °C reveals no weight loss and the final solid holds a weight of 29.9% of the total sample. For **5**, a TG curve also displays two weight losses. The first weight loss of 60.89% from 190 to 245 °C corresponds to the loss of organic components (calcd 60.92%), while the second weight loss of 11.93% from 224.1 to 323.6 °C corresponds to the decomposition of copper oxalate. Complex **4** is thermally stable upon heating to *ca.* 180 °C followed by three stages of weight loss peaking at 198 °C, 277 °C and 334 °C, corresponding to the exclusion of mpz ligands and then degradation. For **9**, the TG curve indicates that the coordinated water molecules and chloride anions are released in the range 75–188 °C (found 9.08%, calcd 9.65%). The weight loss of 50.40% at 234 °C (in the range 190–245 °C) (calcd 44.0%) corresponds to the loss of a N-donor ligand. For **3**, the TG curve indicates that the organic ligands are released in the range 140–260 °C (found 53.3%, calcd 53.4%). The final mass remnant is 23.43% of the total sample.

Magnetic properties and EPR spectra

Magnetic parameters and magnetization data as well as EPR results of the discussed compounds are presented in Table 3. The variation of the magnetization *M versus* the magnetic field *H* has been measured for all complexes at 2 K. The EPR results of **1–9** indicated signals typical for Cu(II) centers in different coordination spheres, like single, axial or rhombic type signals.

Magnetic susceptibility studies indicated that five compounds **2**, **4**, **7**, **8** and **9** revealed the one-dimensional infinite chains of copper(II) centers.

Two methods of calculation of exchange parameters have been used *e.g.* Ising (1)[16] and Fisher (2)[17] models. The Ising model with a molecular field correction was solved for spin $S = 1/2$ for a linear chain system[16] and the Hamiltonian used was:

$$H = -2J\sum_{i=1}^{N} S_i^z S_{i+1}^z + g\beta\sum_{i=1}^{N} HS_i^z + g\beta\sum_{i=1}^{N} H_i^S S_i^z$$

where J is the exchange parameter, N is the number of magnetic atoms, S_i^z is the projection of the spin angular momentum in the direction of quantization, β is the Bohr magneton, H is the external magnetic field, and H_i^S is the molecular field on the i-th atom which describes the interactions between atoms in different chains.

The magnetic susceptibility for such a system is given by the relationship:

$$\chi_M = \frac{N\beta^2 g^2}{4kT} e^{J/kT} \quad (1)$$

which is the one-dimensional Ising model for $S = 1/2$.

In order to obtain values for those exchange parameters, the present data have been fit using also Fisher's classical Heisenberg results[17] for infinite linear chains. A molecular field approximation has been used to account for the interaction between chains. Fisher's equation for the magnetic susceptibility of a classical spin S chain is:

$$\chi_M = \frac{Ng^2\beta^2 S(S+1)}{3kT}\frac{1-u}{1+u} \quad (2)$$

where $u = \coth[2JS(S+1)/kT] - kT/[2JS(S+1)]$ and J is the intrachain exchange parameter.

If there are interactions between chains, the actual observed susceptibility may then be obtained using the results of a molecular field correction:[18]

$$\chi_M^{corr} = \frac{\chi_M}{1 - \frac{2zJ'\chi_M}{Ng_{av}^2\beta^2}} \quad (3)$$

Table 3 Magnetic parameters, magnetization data[a] and EPR data

Compounds	Diamagnetic corrections[b] × 10^6 (cm^3 mol^{-1})	Effective magnetic moments[c] μ_B (B.M.)	Curie constant[d] C (cm^3 K mol^{-1})	Weiss constant[d] Θ (K)	Magnetization[e] (B.M.)	Factors g T = 77 K		T = 293 K	
1	−18	1.38	—	—	0.01	$g = 2.16_0$	Single line	$g = 2.14_5$	Single isotropic line
2	−111	1.84	0.419	−0.24	0.97	$g_\perp = 2.07_3$ $g_\parallel = 2.29_3$	Axial line	$g_\perp = 2.07_6$ $g_\parallel = 2.28_8$	Axial line
3	−109	1.96	0.444	−0.46	0.97	$g_1 = 2.20_6$ $g_2 = 2.11_9$ $g_3 = 2.04_6$	Rhombic line	$g = 2.13_4$ δ_{Hpp} = 138 G	Single isotropic line
4	−102	1.81	0.413	−0.01	0.98	$g = 2.16_0$ δ_{Hpp} = 215 G	Single isotropic line	$g = 2.14_3$ δ_{Hpp} = 107 G	Single isotropic line
5	−117	1.88	0.444	0.74	1.01	$g_\perp = 2.05_5$ $g_\parallel = 2.31_9$	Axial line	$g_\perp = 2.07_7$ $g_\parallel = 2.32_2$	Axial line
6	−61	1.70	—	—	0.01	$g_1 = 2.31_8$ $g_2 = 2.08_1$ $g_3 = 2.03_6$	Rhombic line	$g_\perp = 2.10_8$ $g_\parallel = 2.28_3$	Axial line
7	−75	1.90	0.437	−0.14	0.99	$g = 2.12_5$ δ_{Hpp} = 159 G	Single isotropic line	$g = 2.10_3$ δ_{Hpp} = 164 G	Single isotropic line
8	−51	1.81	—	—	0.15	$g = 2.13_9$ δ_{Hpp} = 215 G	Single isotropic line	$g = 2.13_2$ δ_{Hpp} = 251 G	Single isotropic line
9	−74	1.68	0.346	−2.29	0.56	$g_\perp = 2.04_0$ $g_\parallel = 2.30_4$	Axial line	$g_\perp = 2.07_4$ $g_\parallel = 2.31_5$	Axial line

[a] Data per one copper centre. [b] Including Nα (Cu^{2+}) = 60 × 10^{-6} cm^3 mol^{-1}. [c] At 300 K. [d] In the temperature range 1.8–300 K. [e] At the magnetic field 5 T and temperature 2 K.

where J' is the interaction between chains and z is the number of nearest neighbor chains.

The results of magnetic parameters calculated are presented in Table 4.

Magnetic behavior of compound **8** indicates overall antiferromagnetic interactions among the Cu(II) centers. Upon cooling compound **8** the $\chi_M T$ value shows a linear decrease from 0.404 cm^3 mol^{-1} K (μ_{eff} = 1.81 B.M.) at 300 K up to 0.269 cm^3 mol^{-1} K (μ_{eff} = 1.47 B.M.) at 120 K. The $\chi_M T$ value declines abruptly upon further cooling and reaches a minimal value of 0.058 cm^3 mol^{-1} K (μ_{eff} = 0.68 B.M.) at 1.8 K. Ising and Fisher models were used for calculation of exchange parameters (Table 4).

The evaluated J for compound **8** well correlates with values reported for analogous compounds, $\{[Cu_2(C_2O_4)_2(ampy)_3]\cdot(ampy)\}_n$ (J = −66.6 cm^{-1}; ampy = 2-amino-4-methylpyridine),[19] [(dien)-$Cu(C_2O_4)Cu(H_2O)_2$(tmen)][ClO_4] (J = −75.0 cm^{-1}; tmen = *N*,*N*,*N*′,*N*′-tetramethylethylenediamine, dien = diethylenetriamine)[20] and $\{[Cu(C_2O_4)(H_2O)(3Meade)]\cdot H_2O\}_n$ (J = −34 cm^{-1}; 3Meade = 3-methyladenine).[21] In all these compounds, the oxalato bridging ligand forms two short Cu–O bonds at one copper atom and one short and one long bond at the other copper atom. As a result, one of the metal magnetic orbitals ($d_{x^2-y^2}$ in a tetragonally elongated octahedral geometry) is coplanar with the oxalate bridge, whereas the other one is perpendicular to it. For this topology, the overlap between the magnetic orbitals occurs only *via* one of the two OCO fragments leading to antiferromagnetic coupling. The magnitude of magnetic coupling in such compounds is predicted to be about one-fourth of that observed for the topology with the symmetric bis-bidentate bridging ligand coplanar with the metal magnetic orbital and four short Cu–O_{ox} bond distances, which guarantee the strongest antiferromagnetic couplings (values of J ranging from −260 to −400 cm^{-1}).[23] To some extent the antiferromagnetic interactions in **8** is weakened by different coordination environments of copper of Cu(1) and Cu(2) ions.[22]

The results of magnetic measurements concerning **2**, **4** and **7** compounds show infinite chains in the crystal structure and

Table 4 Magnetic parameters of infinite chains

Compounds	Intrachain parameter J (cm^{-1})	Interchain interaction zJ' (cm^{-1})	Factors g
$[Cu(C_2O_4)(apz)_2]_n\cdot(3H_2O)_n$ (**2**)[a]	−0.12[c] −0.11[d]	−0.10[c] −0.11[d]	2.11_3[c] 2.11_3[d]
$[Cu(C_2O_4)(mpz)_2]_n$ (**4**)[a]	−0.36[c] −0.37[d]	0.83[c] 0.86[d]	2.09_7[c] 2.09_7[d]
$[Cu(C_2O_4)(ampy)(H_2O)]_n$ (**7**)[a]	0.00[c] 0.00[d]	−0.19[c] −0.19[d]	2.15_8[c] 2.15_8[d]
$\{[Cu_2(\mu\text{-}C_2O_4)(aepy)_2][Cu(C_2O_4)_2(H_2O)_2]\}_n\cdot(2H_2O)_n$ (**8**)[b]	−58.9[c] −62.3[d]	0.00[c] 0.00[d]	2.37_9[c] 2.39_9[d]
$[Cu_4(\mu\text{-}C_2O_4)_3(aepy)(H_2O)_2]Cl_2$ (**9**)[a]	−0.35[c] −0.34[d]	−2.39[c] −2.42[d]	1.92_1[c] 1.92_2[d]

[a] Calculated in the temperature range 1.8–300 K. [b] Calculated in the temperature range 120–300 K. [c] Calculated in the temperature range 120–300 K using the Ising model. [d] Calculated in the temperature range 120–300 K using the Fisher model.

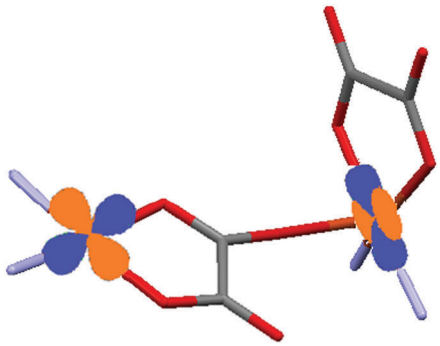

Scheme 3 Orbital topology found in **2**, **4** and **7** and related μ-oxalato-1κ^2O^1,O^2:2κO^{1a}-bridged Cu(II) complexes.

indicate very weak intra- and interchain interactions between copper(II) centers. So far, only several μ-oxalato-1κ^2O^1,O^2:2κO^{1a}-bridged Cu(II) complexes have been magneto-structurally characterized and in almost all previously discussed compounds, including ours, the magnetic orbitals adopt the relative geometry shown in Scheme 3. This configuration is unfavourable for transmitting exchange coupling.[23]

Determination of exchange parameters of dinuclear complexes **1** and **6** was made by fitting the experimental results to the modified Bleaney–Bowers expression (4):[24]

$$\chi_{Cu}^{corr} = \frac{N\beta^2 g_{av}^2}{3kT}\left[1 + \frac{1}{3}\left(e^{-2J/kT}\right)\right]^{-1}(1-x) + \left(\frac{N\beta^2 g_{imp}^2}{4kT}\right)x \quad (4)$$

where χ_{Cu}^{corr} is molar magnetic susceptibility corrected for diamagnetism and t.i.p., calculated per copper(II) magnetic center, N – Avogadros number, k – Boltzmann constant, g_{av} – average g factor, x – percentage of monomeric form of a complex, g_{imp} – g factor of monomeric form of the complex and J is the exchange parameter in the Heisenberg–Dirac–Van Vleck Hamiltonian $\hat{H} = -2J\hat{S}_1\hat{S}_2$.

The relationship of magnetic susceptibility *vs.* temperature for **1** and **6** compounds indicated the presence of paramagnetic impurity (Table 5).

Although the coordination structure of the compounds **1** and **6** is two- and one-dimensional, respectively, from a magnetic point of view, these systems can be considered as dimers. The zigzag polymeric chain of **6** is built up of the $[Cu_2(C_2O_4)_2(bpzm)_2]$ entities. In turn, there are two independent oxalate anions adopting different coordination modes μ-oxalato-1κ^2O^1,O^2:2κ^2O^{1a},O^{2a} and μ$_4$-oxalato-1κ^2O^1,O^2:2κO^1:3κO^{1a},O^{2a}:4κO^{2a} in structure **1** (Fig. 1b). The first one, leading to an almost planar Cu–C_2O_4–Cu framework with four short Cu–O, favours strong antiferromagnetic interactions, whereas the exchange coupling through the out-of-plane exchange pathway μ$_4$-oxalato-1κ^2O^1,O^2:2κO^1:3-κO^{1a},O^{2a}:4κO^{2a} is expected to be very weak.[25]

For calculation of magnetic parameters for compound **5**, Pad'e expression series (5)[26] for the (S = 1/2) Heisenberg model with a molecular field correction (3)[18] was used:

$$\chi_M = \frac{N\beta^2 g^2}{4kT}\left(\frac{L}{M}\right)^{\frac{2}{3}} \quad (5)$$

where

$L = 1 + 5.7979916K + 16.902653K^2 + 29.376855K^3 + 29.832959K^4 + 14.036918K^5$

$M = 1 + 2.7979916K + 7.0086780K^2 + 8.6538644K^3 + 4.5743114K^4$

$K = J/2kT$

The relationship of $\chi_M T$ *vs.* T of the compound increase upon cooling up to a maximal value equal to 0.678 cm^3 mol^{-1} K at 1.8 K.

Magnetic susceptibility data for compound **5** are between 1.8–300 K calculated using the Curie–Weiss expression; Curie constant C = 0.444 cm^3 mol^{-1} K and Weiss constant Θ = 0.74 K. The positive Weiss constant confirms existence of the ferromagnetic coupling between copper(II) centers. The least-squares fit of the experimental data using these equations was limited to the temperature range from 1.8 K up to 300 K and yields J = 1.17 cm^{-1} zJ' = −0.21 cm^{-1} and $g = 2.15_1$ with the agreement factor R equal to 2.73× 10^{-5}.

The weak ferromagnetic coupling observed for compound **5** is in good agreement with the magnetic results reported for related one-dimensional Cu(II) structure based on asymmetric bischelating oxalate bridges with perpendicular topology (where the metal-centered magnetic orbitals are parallel to each other and perpendicular to the oxalato) and angle β (the bond angle C–O–Cu involving the apical oxalate–oxygen) below 109.5° (108.6° in structure **5**), for example in $[Cu(C_2O_4)(bpa)]_n$ (J = +2.50 cm^{-1}; β = 106.9°; bpa = 1,2-bis(4-pyridyl)ethane), $[Cu(C_2O_4)(2\text{-ampy})_2]_n$ (J = +2.00 cm^{-1}; β = 107.8°; 2-ampy = 2-aminopyridine); and $[Cu(C_2O_4)(bipy)]_n$ (J = +2.4 cm^{-1}; β = 108.4°).[25a] The relationship of $\chi_M T$ *vs.* T of compounds **1**, **5** and **6** is presented in Fig. 10.

The Bleaney–Bowers expression (4)[24] of magnetic interaction was also used for calculation of the exchange parameter of semi-dimer **3**.

Table 5 Magnetic parameters of dinuclear-based compounds

Compounds	Exchange parameter J[a] (cm^{-1})	Monomeric form[a] (%)	Factors[b] g	Agreement factor R
$[Cu(C_2O_4)(pz)]_n$ (**1**)	−156	0.94	$g_a = 2.16_0$ $g_b = 2.14_5$	1.98×10^{-5}
$[Cu_2(C_2O_4)_2(bpzm)_2]_n\cdot(3.5H_2O)_n$ (**6**)	−41	0.75	$g_a = 2.16_6$ $g_b = 2.08_5$	2.72×10^{-5}
$[Cu_2(\mu\text{-}C_2O_4)_2(H_2O)_2(ampz)_4]$ (**3**)	−0.45	0.00	$g_a = 2.16_9$ g_b = —	1.31×10^{-4}

[a] Calculated in the temperature range 1.8–300 K. [b] g_a – factor of dimeric form; g_b – factor of monomeric form.

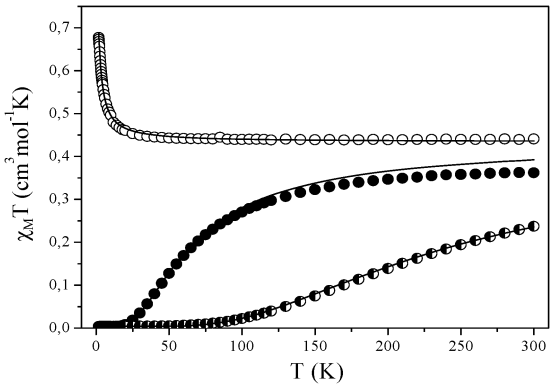

Fig. 10 Thermal dependencies of $\chi_M T$ for compounds **1** (◑), **5** (○) and **6** (●). Experimental magnetic data plotted as $\chi_M T$ (○) *versus* *T*. The solid line is the calculated curve for $\chi_M T$ *vs.* *T*.

Compound **3** indicated a very weak antiferromagnetic coupling of Cu^{2+} centers $J = -0.45$ cm^{-1}, $zJ' = 0$ and $g = 2.16_9$ with the agreement factor *R* equal to 1.32×10^{-4} and indicated lack of any monomeric impurities.

Analysis of magneto-structural data for **1–9** confirmed that the value and type of the magnetic coupling are essentially governed by the magnitude of the overlap between the metal-centered magnetic orbitals ($d_{x^2-y^2}$ orbital in square pyramidal or elongated octahedral geometries) and the highest occupied molecular orbitals of the oxalato ligand. The strongest antiferromagnetic coupling occurs when the oxalato bridge is symmetrically coordinated with two short bond distances at neighboring copper(II) atoms, and it is coplanar with the magnetic orbitals. The equatorial–axial coordination mode of the oxalate bridge with long Cu–O_{ox} bonds substantially reduced the magnetic coupling of copper centers.

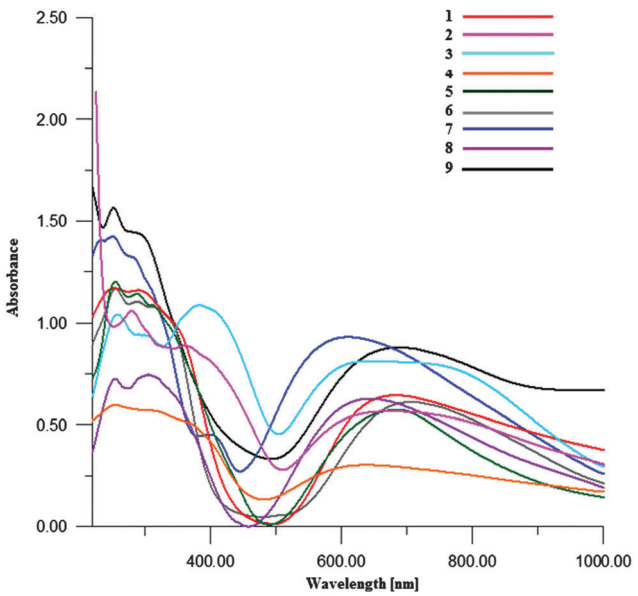

Fig. 11 The electronic reflectance spectra of **1–9**.

Table 6 Electronic spectral data of Cu(II) complexes

Complex	λ_{max} [nm]
$[Cu(C_2O_4)(pz)]_n$ (**1**)	725.0; 300.5; 257.0
$[Cu(C_2O_4)(apz)_2]_n \cdot (3H_2O)_n$ (**2**)	680.0; 403.0; 362.5; 280.0
$[Cu_2(\mu\text{-}C_2O_4)_2(H_2O)_2(ampz)_4]$ (**3**)	742.0; 626.0; 384.0; 294.0; 260.0
$[Cu(C_2O_4)(mpz)_2]_n$ (**4**)	637.0; 373.0; 316.0; 255.0
$[Cu(C_2O_4)(aind)_2]_n$ (**5**)	697.5; 312.5; 288.5; 254.5
$[Cu_2(C_2O_4)_2(bpzm)_2]_n \cdot (3.5H_2O)_n$ (**6**)	710.5; 317.0; 287.5; 255.0
$[Cu(C_2O_4)(ampy)(H_2O)]_n$ (**7**)	611.0; 404.5; 285.0; 251.5; 233.5
$\{[Cu_2(\mu\text{-}C_2O_4)(aepy)_2]\ [Cu(C_2O_4)_2(H_2O)_2]\}_n \cdot (2H_2O)_n$ (**8**)	647.0; 303.0; 256.0
$[Cu_4(\mu\text{-}C_2O_4)_3(aepy)(H_2O)_2]Cl_2$ (**9**)	679.5; 293.5; 251.5

UV-Vis properties

Except for **3**, the electronic reflectance spectra of the examined compounds are characterized by a very broad asymmetric band in the region 600–1000 nm typical for overlapping $d_{xy} \rightarrow d_{x^2-y^2}$, d_{yz}, $d_{xz} \rightarrow d_{x^2-y^2}$ and $d_{z^2} \rightarrow d_{x^2-y^2}$ transitions between d orbitals in tetragonal six or five coordinate Cu(II) complexes with the $d_{x^2-y^2}$ ground state (Fig. 11). The greater is the tetragonality of the complex (the longer the axial bonds), the more shifted to the blue is the low energy absorption maximum. The electronic diffuse reflectance spectrum of **3** exhibits two bands at 742 and 626 nm assigned to $d_{z^2} \rightarrow d_{x^2-y^2}$ and d_{xy}, d_{yz}, $d_{xz} \rightarrow d_{x^2-y^2}$, respectively, and it is also consistent with the elongated tetragonal distortion. Besides the d–d bands, the spectra display bands assigned to LMCT, LLMC and IL transitions. Electronic spectral data for the compounds **1–9** are summarized in Table 6.

Conclusions

In summary, we have successfully synthesized and characterized nine oxalate copper(II) complexes. X-ray analysis revealed the key role of the N-containing auxiliary ligand in the determination of the oxalate coordination mode and final complex architecture. The two dimensional network is formed only in the case of the compound containing the pyrazole ligand. The introduction of substituents into the pyrazole ring increases the complexation properties of N-donor ligands leading to coordination of two ligand molecules and formation of the lower dimensional networks. The exchange interaction between the copper ions *via* the oxalate bridge has been shown to be strongly dependent on the geometry around the Cu ions, the orientation of the magnetic orbitals in respect of the oxalate plane and the bridging mode of the oxalate group. The strongest antiferromagnetic couplings were confirmed for compound $[Cu(C_2O_4)(pz)]_n$ (**1**) in which the oxalato bridge is symmetrically coordinated with two short bond distances at neighboring copper(II) atoms and it is coplanar with the magnetic orbitals. The equatorial–axial coordination mode of the oxalate bridge with long Cu–O_{ox} bonds, detected in other examined structures, substantially reduced the magnetic coupling of copper centers.

Experimental

Materials and general methods

Bis(pyrazol-1-yl)methane was synthesised according to the literature method.[27] The other reagents used for the synthesis were commercially available and were used without further purification. IR spectra were recorded on a Nicolet Magna 560 spectrophotometer in the spectral range 4000—400 cm^{-1} with the samples in the form of KBr pellets. The solid reflectance spectra and UV-Vis spectra were recorded on a Jasco V-630 spectrophotometer in the range 200–1000 nm. EPR spectra were recorded at room temperature and at 77 K on a Bruker Elexsys E 500 spectrometer equipped with an NMR teslameter (ER 036TM) and a frequency counter (E 41 FC) at the X-band. Powder X-ray diffraction (PXRD) measurements were performed on a PANalytical Empyrean X-ray diffractometer using Cu-Kα radiation (λ = 1.5418 Å), in which the X-ray tube was operated at 40 kV and 30 mA ranging from 5 to 80°. Thermogravimetric analysis (TGA) was performed on a Perkin Elmer Pyris1 instrument.

Preparation of 1–9

$(NH_4)_2C_2O_4{\cdot}H_2O$ (0.085 g, 0.60 mmol) was dissolved in water (5 ml) and slowly added to the methanolic solution of $CuCl_2{\cdot}2H_2O$ or $Cu(NO_3)_2{\cdot}3H_2O$ and a suitable N-donor ligand. The resulting solution was kept for evaporation at room temperature, and after a few weeks crystals of **1–9** were obtained, filtered off and dried. Details concerning synthesis of **1–9** are gathered in the table below.

(**1**) $[Cu(C_2O_4)(pz)]_n$: Anal. calc. for $C_5H_4N_2O_4Cu$: C, 27.34; H, 1.84; N, 12.75%. Found: C, 27.68; H, 1.66; N, 12.55%. IR (KBr; cm^{-1}): 3291(s), 3231(m) and 3146(m) ν(NH); 1705(vs) and 1651(vs) ν_{as}(COO); 1602(s) ν(C═N_{pz}) and ν(C═C_{pz}); 1358(s) and 1302(s) ν_s(COO).

(**2**) $[Cu(C_2O_4)(apz)_2]_n{\cdot}(3H_2O)_n$: Anal. calc. for $C_8H_{16}N_6O_7Cu$: C, 25.84; H, 4.34; N, 22.60%. Found: C, 25.99; H, 4.52; N, 22.71%. IR (KBr; cm^{-1}): 3437(s) and 3312(s) ν(NH); 1678(vs) ν_{as}(COO); 1592(m), 1552(m) and 1531(s) ν(C═N_{apz}) and ν(C═C_{apz}); 1429(s) and 1410(sh) ν_s(COO).

(**3**) $[Cu_2(\mu\text{-}C_2O_4)_2(H_2O)_2(ampz)_4]$: Anal. calc. for $C_{20}H_{32}N_{12}O_{10}Cu_2$: C, 33.01; H, 4.43; N, 23.10%. Found: C, 33.40; H, 4.55; N, 23.49%. IR (KBr; cm^{-1}): 3417(s), 3355(s), 3200(s) and 3146(m) ν(NH) and ν(OH); 1673(vs) and 1636(s) ν_{as}(COO); 1595(m), 1578(m) and 1502(m) ν(C═N_{ampz}) and ν(C═C_{ampz}); 1427(s) and 1285(s) ν_s(COO).

(**4**) $[Cu(C_2O_4)(mpz)_2]_n$: Anal. calc. for $C_{10}H_{12}N_4O_4Cu$: C, 38.04; H, 3.83; N, 17.74%. Found: C, 38.39; H, 3.94; N, 17.86%. IR (KBr; cm^{-1}): 3438(m), 3246(m) and 3126(m) ν(NH); 1682(vs) 1661(s) and 1645(s) ν_{as}(COO); 1567(s) and 1521(w) ν(C═N_{mpz}) and ν(C═C_{mpz}); 1414(s) and 1297(s) ν_s(COO).

(**5**) $[Cu(C_2O_4)(aind)_2]_n$: Anal. calc. for $C_{16}H_{12}N_4O_4Cu$: C, 49.55; H, 3.12; N, 14.45%. Found: C, 49.82; H, 3.24; N, 14.66%. IR (KBr; cm^{-1}): 3235(s) ν(NH); 1670(vs) ν_{as}(COO); 1594(s) ν(C═N_{aind}) and ν(C═C_{aind}); 1335(s) and 1311 ν_s(COO).

(**6**) $[Cu_2(C_2O_4)_2(bpzm)_2]_n{\cdot}(3.5H_2O)_n$: Anal. calc. for $C_{18}H_{23}N_8O_{11.5}Cu_2$: C, 32.63; H, 3.50; N, 16.91%. Found: C, 32.97; H, 3.39; N, 17.05%. IR (KBr; cm^{-1}): 3473(br) and 3137(s) ν(OH); 1666(vs) ν_{as}(COO); 1597(s), 1522(w) and 1512(w) ν(C═N_{bpzm}) and ν(C═C_{bpzm}); 1405(s) and 1281(s) ν_s(COO).

(**7**) $[Cu(C_2O_4)(ampy)(H_2O)]_n$: Anal. Calc. for $C_8H_{10}N_2O_5Cu$: C, 34.60; H, 3.63; N, 10.09%. Found: C, 34.95; H, 3.73; N, 10.49%. IR (KBr): 3402(s), 3290(s) and 3139(s) ν(NH) and ν(OH); 1671(vs) and 1652(vs) ν_{as}(COO); 1607(s) and 1571(w) ν(C═N_{ampy}) and ν(C═C_{ampy}); 1435(s) and 1414(s) and 1270(s) ν_s(COO).

(**8**) $\{[Cu_2(\mu\text{-}C_2O_4)(aepy)_2][Cu(C_2O_4)_2(H_2O)_2]\}_n{\cdot}(2H_2O)_n$: Anal. calc. for $C_{20}H_{28}N_4O_{16}Cu_3$: C, 31.15; H, 3.66; N, 7.27%. Found: C, 31.42; H, 3.79; N, 7.51%. IR (KBr): 3312(s), 3248(s) and 3149(s) ν(NH) and ν(OH); 1676(vs) and 1649(vs) ν_{as}(COO); 1618(m), 1595(s) and 1565(sh) ν(C═N_{aepy}) and ν(C═C_{aepy}); 1444(s), 1306(s) and 1293(s) ν_s(COO).

(**9**) $[Cu_4(\mu\text{-}C_2O_4)_3(aepy)_4(H_2O)_2]Cl_2$: Anal. calc. for $C_{34}H_{40}N_8O_{14}Cl_2Cu_4$: C, 36.80; H, 3.63; N, 10.10%. Found: C, 37.08; H, 3.56; N, 10.43%. IR (KBr): 3303(s), 3249(s) and 3149 ν(NH) and ν(OH); 16 775(vs) and 1648(vs) ν_{as}(COO); 1595(s) ν(C═N_{aepy}) and ν(C═C_{aepy}); 1444(s), 1306(s) ν_s(COO).

Crystal structure determination and refinement

The X-ray intensity data for **1–9** were collected on a Gemini A Ultra Oxford Diffraction four-circle kappa geometry diffractometer with Atlas CCD detector graphite monochromated MoK_α radiation (λ = 0.71073 Å) at 293.0(2) K. The unit cell determination and data integration were carried out using the CrysAlis package of Oxford Diffraction.[28] Intensity data were corrected for the Lorentz and polarization effects. The absorption correction was introduced using the SCALE3 ABSPACK scaling algorithm.[28] The structure was solved by direct methods using SHELXS-97 and refined by full matrix least-squares on F^2 using SHELXL-97 with anisotropic displacement parameters for non-hydrogen atoms.[29] The hydrogen atoms were treated as ''riding'' on their parent carbon atoms and assigned isotropic temperature factors equal to 1.2 (non-methyl) and 1.5 (methyl and water) times the value of the equivalent temperature factor of the parent atom. The oxygen atom of one water molecule of compound **6** occupies the inversion centre and thus the hydrogen atoms of these molecules are disordered at two positions by symmetry. Because the local electron density maximum smaller than 0.5 e $Å^{-3}$ cannot be reliably determined by X-ray diffractometry, this water molecule disordered hydrogen atoms were not included into refinement. The Cu2 atom in compound **8** shows signs of prolation. The introduction of the multipositional disorder model to this atom does not lead to improvement of the displacement parameters, *i.e.* all partially occupied domains also exhibit prolation with the major axis pointing in the same direction as existing for non-disordered one. Thus it can be supposed that the observed disorder is dynamic in character. It must be noted that the major axis of prolating ellipsoid is located along the bonds elongated as a consequence of the Jahn–Teller effect, thus the longer and consequently the weaker bonds allow a larger displacement in their direction. The ethylamine moiety of the one 2-(2-pyridyl)ethylamine ligand of compound **9** is disordered equally over two sites. Crystal data collection and refinement parameters are summarized in Table 1. The hydrogen bonds

and selected bond distances and angles of **1–9** are listed in Tables S1–S10 (ESI†).

Magnetic measurements

Magnetic measurements in the temperature range 1.8–300 K were performed using a Quantum Design SQUID-based MPMSXL-5-type magnetometer. The SQUID magnetometer was calibrated using the palladium rod sample (Materials Research Corporation, measured purity 99.9985%). The superconducting magnet was generally operated at a field strength ranging from 0 to 5 T. Measurements were made at a magnetic field of 0.5 T. Corrections are based on subtracting the sample – holder signal and contribution χ_D estimated from the Pascal constants.[30] Magnetization measurements were conducted at 2 K at the magnetic field from 0 to 5 Tesla.

Acknowledgements

This research was supported by the National Science Centre (Poland) under grants No. 2011/03/N/ST5/04421 and No. 2011/01/B/ST5/01624.

References

1 (*a*) S. A. Barnett and N. R. Champness, *Coord. Chem. Rev.*, 2003, **246**, 145; (*b*) O. Kahn, *Molecular Magnetism*, VCH, New York, 1993; (*c*) A. M. Beatty, *Coord. Chem. Rev.*, 2003, **246**, 131; (*d*) B.-H. Ye, M.-L. Tong and X.-M. Chen, *Coord. Chem. Rev.*, 2005, **249**, 545; (*e*) A. Y. Robin and K. M. Fromm, *Coord. Chem. Rev.*, 2006, **250**, 2127; (*f*) S. Kitagawa and R. Matsuda, *Coord. Chem. Rev.*, 2007, **251**, 2490; (*g*) W. K. Chan, *Coord. Chem. Rev.*, 2007, **251**, 2104; (*h*) R. L. LaDuca, *Coord. Chem. Rev.*, 2009, **253**, 1759; (*i*) A. Morsali and M. Y. Masoomi, *Coord. Chem. Rev.*, 2009, **253**, 1882; (*j*) W. Lee Leong and J. J. Vittal, *Chem. Rev.*, 2011, **111**, 688; (*k*) Ch.-L. Ho and W.-Y. Wong, *Coord. Chem. Rev.*, 2011, **255**, 2469.

2 (*a*) L. Yi, X. Yang, T. Lu and P. Cheng, *Cryst. Growth Des.*, 2005, **5**, 1215; (*b*) T. Liu, J. Lu and R. Cao, *CrystEngComm*, 2010, **12**, 1489; (*c*) W. Jia, J. Luo and M. Zhu, *Cryst. Growth Des.*, 2011, **11**, 2386; (*d*) Y. Y. Karabach, A. M. Kirillov, M. Haukka, J. Sanchiz, M. N. Kopylovich and A. J. Pombeiro, *Cryst. Growth Des.*, 2008, **8**, 4100; (*e*) A. M. Kirillov, *Coord. Chem. Rev.*, 2011, **255**, 1603; (*f*) J. Tong, S.-Y. Yu and H. Li, *Chem. Commun.*, 2012, **48**, 5343.

3 (*a*) M. Hernández-Molina, P. A. Lorenzo-Luis and C. Ruiz-Pérez, *CrystEngComm*, 2001, **16**, 1; (*b*) P. S. Mukherjee, S. Konar, E. Zangrando, C. Diaz, J. Ribas and N. R. Chaudhuri, *J. Chem. Soc., Dalton Trans.*, 2002, 3471; (*c*) X.-Y. Song, L.-C. Li, D.-Z. Liao, Z.-H. Jiang and S.-P. Yan, *Cryst. Growth Des.*, 2007, **7**, 1220; (*d*) A. Recio, J. Server-Carrió, E. Escrivá, R. Acerete, J. García-Lozano, A. Sancho and L. Soto, *Cryst. Growth Des.*, 2008, **8**, 4075; (*e*) T. C. Stamatatos, S. P. Perlepes, C. P. Raptopoulou, V. Psycharis, C. S. Patrickios, A. J. Tasiopoulos and A. K. Boudalis, *Inorg. Chem. Commun.*, 2009, **12**, 402–405; (*f*) S. Youngme, G. A. van Albada, N. Chaichit, P. Gunnasoot, P. Kongsaeree, I. Mutikainen, O. Roubeau, J. Reedijk and U. Turpeinen, *Inorg. Chim. Acta*, 2003, **353**, 119; (*g*) A. Bentama, O. Schott, J. Ferrando-Soria, S.-E. Stiriba, J. Pasán, C. Ruiz-Pérez and M. Julve, *Inorg. Chim. Acta*, 2012, **389**, 52–59.

4 C. F. Macrae, I. J. Bruno, J. A. Chisholm, P. R. Edfinfton, P. McCabe, E. Pidcock, L. Rodriguez-Monge, R. Taylor, J. van de Streek and P. A. Wood, *J. Appl. Crystallogr.*, 2008, **41**, 466.

5 (*a*) A. Gleizes, M. Julve, M. Verdaguer, J. A. Real, J. Faus and X. J. Solans, *J. Chem. Soc., Dalton Trans.*, 1992, 3209; (*b*) Y. Akhriff, Y. J. Server-Carrió, A. Sancho, J. García-Lozano, E. Escrivá, J. V. Folgado and L. Soto, *Inorg. Chem.*, 1999, **38**, 1174.

6 K. Nakamoto, *Infrared and Raman Spectra of Inorganic and Coordination Compounds*, Wiley-Interscience, New York, 4th edn, 1986.

7 (*a*) G. A. Jeffrey and W. Saenger, *Hydrogen Bonding in Biological Structures*, Springer-Verlag, 1994; (*b*) G. R. Desiraju and T. Steiner, *The Weak Hydrogen Bond in Structural Chemistry and Biology*, Oxford University Press, 1999.

8 A. Recio, J. Server-Carrió, E. Escrivà, R. Acerete, J. García-Lozano, A. Sancho and L. Soto, *Cryst. Growth Des.*, 2008, **8**, 4075.

9 V. A. Blatov, A. P. Shevchenko and V. N. Serezhkin, *J. Appl. Crystallogr.*, 2000, **33**, 1193.

10 H. Núñez, J.-J. Timor, J. Server-Carrió, L. Soto and E. Escrivá, *Inorg. Chim. Acta*, 2001, **318**, 8.

11 B. J. Hathaway, in *Comprehensive Coordination Chemistry*, ed. G. Wilkinson, Pergamon, Oxford, 1985, vol. 5, p. 604.

12 F. H. Allen, *Acta Crystallogr., Sect. B: Struct. Sci.*, 2002, **58**, 380.

13 A. W. Addison, T. N. Rao, J. Reedijk, J. Rijn and G. C. Verschoor, *J. Chem. Soc., Dalton Trans.*, 1984, 1349.

14 O. Castillo, A. Luque, F. Lloret and P. Román, *Inorg. Chem. Commun.*, 2001, **4**, 350.

15 O. Castillo, J. Alonso, U. García-Couceiro, A. Luque and P. Román, *Inorg. Chem. Commun.*, 2003, **6**, 803.

16 (*a*) J. W. Stout and R. C. Chisholm, *J. Chem. Phys.*, 1962, **36**, 979; (*b*) B. C. Gerstein, F. D. Gehring and R. D. Willett, *J. Appl. Phys.*, 1972, **43**, 1932.

17 M. E. Fisher, *Am. J. Phys.*, 1964, **32**, 343.

18 J. S. Smart, *Effective Field Theories of Magnetism*, W.B. Saunders Comp., Philadelphia and London, 1966.

19 O. Castillo, A. Luque, M. Julve, F. Lloret and P. Román, *Inorg. Chim. Acta*, 2001, **315**, 9.

20 M. Julve, M. Verdaguer, O. Kahn, A. Gleizes and O. Philoche-Levisalles, *Inorg. Chem.*, 1984, **23**, 3808.

21 S. Pérez-Yáñez, O. Castillo, J. Cepeda, J. P. García-Terán, A. Luque and P. Román, *Inorg. Chim. Acta*, 2011, **365**, 211.

22 L. Zhang, W.-M. Bu, S.-P. Yan, Z.-H. Jiang, D.-Z. Liao and G.-L. Wang, *Polyhedron*, 2000, **19**, 1105.

23 T. D. Keene, H. R. Ogilvie, M. B. Hursthouse and D. J. Price, *Eur. J. Inorg. Chem.*, 2004, 1007.

24 B. Bleaney and K. D. Bowers, *Proc. R. Soc. A*, 1952, **214**, 451.

25 (*a*) U. García-Couceiro, O. Castillo, A. Luque, J. P. García-Terán, G. Beobide and P. Román, *Cryst. Growth Des.*, 2006,

8, 1839–1847; (*b*) J. P. García-Terán, O. Castillo, A. Luque, U. García-Couceiro, P. Román and F. Lloret, *Inorg. Chem.*, 2004, **43**, 5761.
26 G. A. Baker Jr, G. S. Rushbrooke and H. E. Gilbert, *Phys. Rev.*, 1964, **135**(5), 1272.
27 E. Díez-Barra, A. de la Hoz, A. Sánchez-Migallón and J. Tejeda, *Heterocycles*, 1992, **34**, 1365.
28 *CrysAlis RED, Version 1.171.29.2.*, Oxford Diffraction Ltd.; G. M. Sheldrick, *Acta Crystallogr., Sect. A: Found. Crystallogr.*, 1990, **46**, 467.
29 G. M. Sheldrick, *Acta Crystallogr., Sect. A: Found. Crystallogr.*, 2008, **64**, 112.
30 E. König, *Magnetic Properties of Coordination and Organometallic Transition Metal Compounds*, Springer, Berlin, 1966.

